Referee #1:

We thank the referee for the constructive comments which will provided a helpful basis for the revision of our ms in due course. Below, we address the main points raised by referee #1.

As to the concepts we aim to present in our ms, many of the comments have shown us that, rather than being in disagreement with the views of referee #1, we did not arrive at articulating some of them clearly enough. Our answers below strive to clarify our concepts better and resolve some of the perceived disagreements.

Referee comment: Otter and colleagues exposed specimens of a veneroid bivalve from Australia to episodically strongly elevated Sr levels (18 times above normal marine levels) in order to make the shell growth visible. They studied the effect of high Sr levels in the water on shell ultrastructure, crystallographic orientation, shell chemistry and growth rate. Except for the shell chemistry, all above mentioned shell properties remained unchanged. Sr/Ca values in the shell increased proportionately to that in the water, i.e. ca. 18 times, which still is way below expected thermodynamic equilibrium, a result supporting previous studies. Findings were interpreted to indicate an "intracellular, diffusion driven, selective transport" of ions across the mantle epithelium and subsequent shell formation processes via amorphous calcium carbonate.

The experiment and analyses were superbly executed and I really enjoyed reading the results. A broad variety of different machines (EBSD, nanoSIMS, μRaman spectroscopy, EPMA, TGA, optical microscopy and FEG-SEM) were employed to study physical and chemical properties of the shells. Yet, the study contains a number of flaws that need to be addressed in a significantly revised version of the ms.

Referee comment: (1) Authors need to specify the overarching goals of their study more clearly and formulate specific hypotheses. For example, I do not think that the main goal was just "to visualize growth" with Sr labeling as stated in the first (= most important) sentence of the Abstract. The title lists at least two other topics. In contrast to the great data presented in this manuscript, the Abstract and Introduction are very weak, poorly structured and organized, and the overarching (and far-reaching) purpose of the study remains elusive. The text is full of juxtapositions, i.e., sentences and paragraphs need better transition. In the Abstract, actual numbers of key data must be given, i.e., the 18 times enrichment in the shell (at least in the outer portion thereof; see below) following exposure to 144 μg/g Sr instead of 8μg/g (translate these data into molar Sr/Ca ratios, please). In the Introduction, authors should first place their study into broader context and identify the motivation for this investigation (which is not that existing in-situ staining methods affect the physiology of bivalves! See below). They need to describe open research questions and how they were addressed here. At the end of the Introduction and later in the Conclusions section, authors need to describe the implications of their finding, e.g., that bivalves likely serve as faithful recorders of the ocean chemistry etc. (which essentially emerges from the observation that Sr/Cashell changes proportionately to Sr/Ca_{shell} if the Sr_{water} level is increased, or, as the authors expressed it – an interesting point of view by the way – irrespective of the Sr level of the water, Ca_{shell}/Ca_{water} and Sr_{shell}/Sr_{water} remained the same).

Answer: As outlined in our introductory paragraph above, we agree with the referee that both abstract and introduction could have provided a better focus on the topics and research questions the ms touches on and we have edited these sections accordingly. Some of the misunderstandings below could have been avoided and have been clarified in the revised version of the ms. Contrary to what the referee may think, it is indeed the overarching goal of this ms to characterize shell architecture and growth at the submicron scale via visualization using Sr-pulse labelling. It is, on the other hand, only natural that this approach enables study and discussion of related aspects that are incorporated into this manuscript and that are therefore also mentioned in the abstract. We now provide numbers in the abstract and molar Sr/Ca ratios. We are aware that molar Sr/Ca ratios are frequently used in sclerochronology, however, this is not the case for biomineralization, geochemistry, and structural biology.
The increase of Sr in shell calculated by the reviewer are in fact incorrect, as these are based on oxide concentrations given in the manuscript and not on element concentrations. We provide now the correct values that result in lower values with 13x (oOSL) and 12x (iOSL) but are still in the same dimension as the 18x assumed by the referee. 12x for the iOSL results also from a minim value as stated in the footnote of table 1. For clarity we added ">" in front of the value within the table. These factors are now also presented in the results and discussion sections together with the new distribution factors, which demonstrate that the system is in disequilibrium compared to the equilibirum partitioning of Sr/Ca during inorganic precipitation of aragonite from seawater as shown by Gaetani & Cohen 2006.

References:

Gaetani, G. A., & Cohen, A. L. (2006). Element partitioning during precipitation of aragonite from seawater: a framework for understanding paleoproxies. Geochimica et Cosmochimica Acta, 70(18), 4617-4634.

Referee comment: (2) Authors erroneously speak of outer and inner shell layer, but, in fact, they have only studied the outer shell layer, which in almost all bivalves is divided into two ultrastructurally different portions, i.e., the outer and inner portion of the outer shell layer (in the following, oOSL and iOSL). The inner shell layer (ISL) is located way back (below what is depicted in Fig. 4C) and (in a cross-sectioned shell) starts where the myostracum intersects with the inner shell surface (= aka pallial line) and ends somewhere at the hinge portion. In Figure 1B, the inner shell layer is formed approx. inside the brown areas, whereas the brown section and portions outside thereof largely belong to the iOSL; the oOSL is likely not seen in this image. The pallial line delimits the ISL from the iOSL. I recommend to look at Fig. 2A in Schöne (2013).

Answer: We are grateful to the referee for pointing out the intricacies of shell nomenclature. We did not mean to use zoological terminology in our ms, but merely strived to apply appropriate terminology to distinguish the structurally inner parts of the shell from the outer parts in the studied area of the shell at the shell tip. While we realize that this may have been misleading, it is not the aim of our study to describe the ultrastructure in its entirety across the shell. Our study targets the area at and along the ventral margin to the outside of the pallial line. We have now clarified this in the new version of the ms and use the appropriate nomenclature in agreement with the morphological elements of a bivalve shell.

Referee comment: (3) Surprisingly, a number of relevant recent papers dealing with very similar issues remain uncited. For example:

(3a) In-situ labeling: Mouchi et al (2013) labeled oysters with manganese to study growth rates, and Mouchi et al. (2016) used immunogold to obtain insights into biomineralization processes of Crassostrea gigas. Riascos et al (2007) tested three different stains in abalone and the surf clam, i.e., calcein, alizarin and strontium chloride.

(3b) Zhao et al (2017a) recently demonstrated that Sr/Ca in the outer shell layer of Corbicula fluminea increases proportionately to Sr/Ca in the ambient water and is not affected by growth rate effects. A very similar finding as reported here.

Answer: ‘Labelling’ methods have been around for decades and provide us with a powerful tool for many different purposes. It is therefore important to refer to the specific purpose rather than to generalize. The papers referred to by the referee above do not at all deal with “very similar issues” and we will clarify this in the revised ms.

The main aim in our study is to use Sr pulse-labelling as a marker to study the structure of the shell at the nano-micro scale. This variety of labelling, termed ‘pulse-labelling’, is an accepted method often used for corals, employing either elemental or enriched isotope spikes (e.g. Brahmi et al., 2012, Domart-Coulon et al., 2014). Pulse-labelling highlights growth features at the micro-nano-scale, which ‘general’ labelling is not able to and, thus, the further has an entirely different focus of study than the latter.

Instead, the labelling studies carried out by Mouchi et al (2013), Riascos et al (2007) as well as of Zhao et al (2017) aimed at growth rate determination at a much lower spatial resolution and the labels were analysed by means of different instrumentation, thus, were not carried out for the same purpose as our study. Similarly, immunogold labelling (Mouchi et al., 2017) is a routine method in protein chemistry used to label functional groups in specific organic molecules present in the shell. Unlike our study, it is carried out ‘ex situ’ and not on living bivalves.

Our speculations on the effect of growth rates on Sr/Ca ratios are a secondary result that warranted discussion, but this topic is in no way the focus of this study. It is interesting to see that our study apparently reproduced the observations of Zhao et al. (2017) on the lack of a growth rate effect on Sr/Ca and we have now referenced this article in the revised version. However, these authors used a very different and taxonomically unrelated bivalve species which, unlike the one we studied, lives in freshwater environments, and has a very different shell architecture. Therefore, this outcome, if correct, is not intuitive.

References for this answer:

Brahmi, C., Domart-Coulon, I., Rougée, L., Pyle, D. G., Stolarski, J., Mahoney, J. J. et al. (2012). Pulsed 86 Sr-labeling and NanoSIMS imaging to study coral biomineralization at ultra-structural length scales. Coral Reefs, 31(3), 741-752.

Domart-Coulon, I., Stolarski, J., Brahmi, C., Gutner-Hoch, E., Janiszewska, K., Shemesh, A., & Meibom, A. (2014). Simultaneous extension of both basic microstructural components in scleractinian coral skeleton during night and daytime, visualized by in situ 86Sr pulse labeling. Journal of Structural Biology, 185(1), 79-88.

Referee comment: (3c) An alternative mechanism of how the bivalve controls the trace and minor element levels in the shell – brought forward by Shirai et al. (2014) and based on Stephenson et al. (2008) – was also ignored: Organic macromolecules near the shell formation front exert control on which and how many ions are incorporated into the carbonate phase of the shells. If the overall production of biomass and thus growth rate decreases (e.g., during times of low food availability), less of such organic substances are produced and the level of trace impurities in the shell carbonate automatically increases. This in turn, affect the morphology of biominerals and likely explains the more primitive ultrastructure at growth annual and even daily growth lines (biochecks) (Füllenbach et al. 2017), i.e., irregular simple/spherulitic prismatic ultrastructure (Schöne 2013). Data in Table 1 also indicate that different microstructures in your study contain different Sr levels, likely for the very reason described above. However, you did not discuss this or the fact that the relative change in the iOSL is only ca. 14 times, not 18.

Answer to 3C discussed by theme:

(2) Growth lines, shell composition and architecture:

In contrast to the referee's statement, reduced growth rates in bivalve shells do not scale to all moieties (mineral and organic) in the shell. Many bivalve species with nacroprismatic shell structure, for example, form an annual growth line that is organic-rich (and poorly mineralized; e.g. Soldati et al., 2008), suggesting that these species independently downregulate the mineralization of the shell from the production of the organic moiety in times of slow growth. These organic-rich shell areas do not contain vastly differing trace element budgets compared to the more mineralized parts of the shell, demonstrating that there is nothing 'automatical' about this process that could be generalized across species. Shells of bivalve species that form a mineralized growth line (e.g. *Arctica islandica*) contain much less overall organic moiety compared to nacroprismatic shells (Non-nacreous: ca. 1-1.5 wt% vs nacreous: 3-5 wt%, Agbaje et al., 2017a, b, 2019). It would be interesting to see any *direct evidence* for a downregulated production of organic components in those bivalve species that form mineralized growth lines, rather than correlative speculation as presented in Füllenbach et al. 2017.

(3) Potential control of the shell architecture by organic macromolecules:

To date, there is no direct evidence for how the complexities of the bivalve shell ultrastructure are connected (if at all) to the composition and amount of organic molecules present in the shell. Instead, it is well known that the composition and amount of the organic moiety in shells varies significantly between species (Agbaje et al., 2017a, b, 2018, 2019, Currey et al 1976, Hare, 1965, Kamat et al 2000) and does so independently of the shell ultrastructure.

Compared to this direct evidence present in the literature, Füllenbach et al. (2017) base their model on how the ultrastructure of bivalve shells relates to the organic moiety on proxy analyses, namely S/Ca ratios in the shell analysed by EPMA. Direct characterization and analysis of the organic molecules in the shells is not presented in their study. Hence, this hypothesis brought forward by the referee is therefore highly speculative and suggestive at best.

(3) Potential control of trace element incorporation into the shell by organic molecules at the shell growth front

This topic is also part of the next referee comment and will be addressed below.

Following the referee's advice, we have incorporated these models developed by Stephenson et al. (2008) and the Schöne group in the revised version of the ms.

References for this answer:

Agbaje, O. B., Thomas, D. E., Mclnerney, B. V., Molloy, M. P., & Jacob, D. E. (2017a). Organic macromolecules in shells of *Arctica islandica*: comparison with nacroprismatic bivalve shells. Marine Biology, 164(11), 208.

Agbaje, O. B. A., Wirth, R., Morales, L. F. G., Shirai, K., Kosnik, M., Watanabe, T., & Jacob, D. E. (2017b). Architecture of crossed-lamellar bivalve shells: the southern giant clam (*Tridacna derasa*, Röding, 1798). Royal Society Open Science, 4(9), 170622.

Agbaje, O.B.A., Ben Shir, I., Zax, D.B., Schmidt, A**.,** Jacob, D.E. (2018) Biomacromolecules within bivalve shells: is chitin abundant? *Acta Biomaterialia* 80, 176-187; 10.1016/j.actbio.2018.09.009

Agbaje, O. B., Thomas, D. E., Dominguez, J. G., Mclnerney, B. V., Kosnik, M. A., & Jacob, D. E. (2019). Biomacromolecules in bivalve shells with crossed lamellar architecture. Journal of Materials Science, 54(6), 4952-4969.

Currey, J. D., & Kohn, A. J. (1976). Fracture in the crossed-lamellar structure of *Conus* shells. Journal of Materials Science, 11(9), 1615-1623.

Hare, P. E. (1965). Amino acid composition of some calcified proteins. Carnegie Inst. Washington Yearbk., 64, 223-232.

Kamat, S., Su, X., Ballarini, R., & Heuer, A. H. (2000). Structural basis for the fracture toughness of the shell of the conch *Strombus gigas*. Nature, 405(6790), 1036.

Referee comment: (4) The alternative mechanism of element incorporation mentioned in 2c does not require any control on uptake of elements. Although the chemical composition of the extrapallial fluids or gels (outer EPF forming the OSL, inner EPF the ISL) of marine bivalves have rarely been measured, the few available studies (e.g., Wada & Fujinuki 1976) unequivocally show that they have nearly the same ionic strength and chemical composition as the ambient seawater (Crenshaw 1972, Lorens & Bender 1980). This is no surprise, because bivalves are osmoconformers, like all other marine organisms. Imagine which energetic efforts were otherwise required if the bivalves had to constantly pump these ions out of the body fluids. Some elements such as strontium, magnesium and sodium reach the body fluids as ions from the ambient water through the gills and the gut (Wilbur & Saleuddin 1983) and across the mantle epithelium (passive diffusion). I have prepared a table for you summarizing data from Wada & Fujinuki (1976) (Table 1).

Table 1. Average element-to-Ca ratios in the inner extrapallial fluid of marine bivalves in comparison to seawater. Calculated from chemical data reported in Wada & Fujinuki (1976).

	Seawater	EPS during growth	EPS during resting
Na/Ca (mol/mol)	44.3	44.1	42.4
Li/Ca (mmol/mol)	2.1	2.6	2.7
Mg/Ca (mol/mol)	5.0	5.1	4.9
Sr/Ca (mmol/mol)	8.3	9.4	8.0
Mn/Ca (mmol/mol)	30.2	291.1	223.9

Despite this, shells are strongly depleted in many trace and minor elements. For example, if measured with a spatial resolution of ca. 50µm Sr/Ca in aragonitic OSL of *Arctica islandica* ranges between ca. 1-3 mmol/mol and Mg/Ca remains below 0.8 mmol/mol (e.g., Schöne et al. 2011). Even when measured by much higher spatial resolution (nanoSIMS) which might be advantageous given the strong chemical heterogeneity of the shell at the µm-scale, Sr/Ca in aragonite of *Cerastoderma edule* does reach values expected for equilibrium fractionation (Füllenbach et al., 2017). In calcitic shells of various species, Mg/Ca ranges between ca. 4-28 mmol/mol (see summary in Vihtakari et al. 2016). These findings lend support to the hypothesis that unwanted elements are actively excluded from the shell by specialized organic macromolecules directly at the site of shell formation (Schöne 2013; Shirai et al. 2014). How this mechanism fits to the ACC-mediated shell formation processes needs to be discussed. Since the chemistry of body fluids of bivalves resembles that of seawater, there is no need for any active transmembrane element transport. Zhao et al. (2017b) recently demonstrated very clearly that Sr, Mg and Ba levels in shells of *Corbicula fluminea* were not transported by active transport mechanisms and did not use the same pathways as Ca. These authors have poisened Ca2+ATPase and blocked Ca2+ channels.

According to the finding by Zhao and colleagues, a passive diffusion pathway across the mantle epithelium is much more likely and would perfectly fit to the incorporation control by organic macromolecules at the shell formation front. I strongly feel that these alternative explanations must be presented and discussed.

Answer: This section in the submitted version of the ms is very speculative, and this was also pointed out by referee #2. We will follow the advice of referee #2 to omit this section to remain closer to our robust and detailed results. Nevertheless, we welcome this opportunity to reply to the referee's comments above and to correct a number of flaws, inaccuracies and misconceptions articulated by the referee:

Contrary to the referee's statement, not all marine organisms are osmoconformers.

It is generally not helpful in this discussion to use poorly defined terms. This is even more relevant in the fundamentally interdisciplinary field of biomineralization where communication across discipline boundaries relies much on the correct usage of terminology. In this line of thought, terms such as "unwanted elements" which presumably refers to concepts of 'chemical fractionation' and 'incompatibility' rather than to an organism expressing its free will, and the term 'ACC-mediated' for a mechanism that produces metastable ACC as a transient precursor, but by no means as an active player that could actively 'mediate' any given process, are not furthering mutual understanding nor scientific progress.

We note that the biomineralization concepts articulated by the referee as well as in Füllenbach et al (2017) rely mainly on literature from the 1950 to 1980s. While many of the pioneering works in the field we are building on today have indeed been produced in this period of time, the field of biomineralization is very fast moving with rapid progress today being made mainly across chemistry, material sciences and physics. This large body of relevant literature is not captured in the referee's comments. One of the concepts, for instance, that experienced major revision is that of the extrapallial fluid (EPF), whose existence as a fluid with a defined composition is questioned today, to say the least. A valuable summary into the questionable nature and existence of the EPF is given in Marin et al. (2012), who state: "(…) its sampling is tricky. On different occasions, having done ourselves these experiments with a small syringe and a tiny needle on different model organisms, we were never fully convinced that the fluid that we were sampling was the right one! Furthermore, (…) it is likely that the composition of this fluid is not homogeneous, but varies from the central shell zone to the shell edge. Furthermore, it seems that the composition of this fluid also varies according to seasons." Following this reasoning we would challenge the referee's line of thought and suggest that the reason for why the table shows the composition of the EPF to be so similar to seawater is that its major component is indeed seawater, because the extrapallial space most likely is not fully sealed towards the outside.

Lastly, after carefully studying Zhao et al. (2017) we find that the reasoning presented there is mostly correlative and highly speculative, while direct evidence is rarely provided to underpin their interpretation. Furthermore, the study focusses on a freshwater bivalve species with different shell architecture from the species we studied and uses different analytical methods at much lower spatial resolution. As generalization at this level and across species is difficult, we would be interested to learn the reasons for how the results of this study would be relevant for our work and why the apparent agreement between a subset of our results with those of Zhao et al. (2017) would be more than a coincidence. Although we have significantly shortened and rewritten this section we were happy to reference Zhao et al. (2017).

References for this answer:

Marin, F., Le Roy, N., & Marie, B. (2012). The formation and mineralization of mollusk shell. Front Biosci, 4(1099), 125.

Referee comment: (5) Another argument against ATP-mediated uptake mechanism is unchanged growth rate of the bivalve. If the hypothesis by Otter and colleagues holds true according to which an "intracellular, diffusion driven, selective transport" of ions is responsible for the observed low Sr shell concentrations, then it is surprising that shell growth rate remained unchanged. A selective transport consumes energy = ATP), and the energy demand for such a transport process increases if the Sr level in the water rises. If more energy is devoted to the control of Sr incorporation into the shell, less energy is available for shell formation resulting in lower growth rate.

Answer: Metabolic processes regulating shell growth are complex and not yet fully understood. It is an interesting and intuitive suggestion by the referee that ATP driven transport results in lower growth rates. However, without direct evidence, there is no way to test this hypothesis. This highlights just how speculative this section of the manuscript was and supports us in the decision to have followed the advice given by referee #2 to cut this section completely.

Referee comment: (6) There is a confusing usage of the term "uptake" (e.g., P2L8). 'Uptake' refers to way elements take from the environment to body fluids. This can either occur through mantle epithelia (in ionic form, potentially by one of the pathways listed in your paper) or during digestion of food. Is this really what you mean here on page 2 or rather the 'incorporation' of elements into the shell at the site of shell formation? From the context, I assume you meant the latter: "Recent studies showed that the uptake of some trace elements, such as strontium, are strongly influenced by crystal growth rates, shell curvature and ontogeny in addition to physiological effects".

Answer: We agree with the referee that, to differentiate between 'uptake' from the water and 'incorporation' into the shell, it is more accurate to use 'incorporation' when referring to shell formation and have replaced it as suggested.

Referee comment: (7) A number of observation were only presented, but not discussed and combined with other aspects of the study, e.g., different amounts of organics in different ultrastructures.

Answer: We believe our discussion of the organic contents in different shell architectures is sound and fully based on the evidence provided in the ms.

Referee comment: (8) Interpretation of the timing of shell growth, meaning of microgrowth increments (= daily), major biochecks (= annual) and greyscale changes (= fortnights) is purely speculative and not supported by the data presented. This would require mark-and recovery experiments. Though not unlikely that the regular change in greyscale results from fortnightly changes, you need to cite at least relevant papers dealing in detail with such tide-controlled growth patterns (Evans 1972, Ohno 1989, Schöne 2008, Hallmann et al. 2009). B the way, you did not say where the bivalves lived: in the intertidal zone? You also noticed that you observed 6 lines in portions formed in tanks during 6 (solar) days suggesting that at least these growth patterns are circadian. However, you have no evidence that the same applies to shell portions formed in nature. Given that the specimens lived in the intertidal zone (please provide details on tidal regime: diurnal or semidiurnal, tidal range etc.), it is reasonable to assume that they have formed circalunidian growth patterns (lunar days). Perhaps, acclimatization to circadian lab conditions were sufficient to reset biological clock resulting tin switch from lunar to solar daily. However, all this needs some discussion (in the Discussion section, not results as currently presented).

Answer: In contrast to what the referee understands, the greyscale patterns in the shells the referee refers to here (Fig. 1D, E) were not formed during aquaculture, but are growth features of the shell formed in the wild before shells were transferred to the aquarium. Our interpretation of these as time gauges for shell growth is therefore valid. We incorporated the tidal regime into the results as well as the materials and methods section. As already stated in the discussion section of the manuscript these bivalves live in the intertidal zone. Suggested relevant literature has been included and the part regarding greyscale line profiles of shell grown in the natural environment has been moved to the discussion as suggested.

Referee comment: (9) Since you are aiming to publish your paper in a journal that is often read by people of the proxy and paleoclimate communities, you need to translate oxide values into element concentrations (as well as molar element/Ca data), and all element/Ca data into molar ratios (required for easier, direct comparison with published data). Likewise, instead of reporting Ca/Sr ratios, please turn this around and give Sr/Ca data.

Answer: Although traditionally EPMA data is presented as wt.% oxide we have moved this table as it is to the supplement and replaced it in the ms with elemental concentrations provided as $\mu g \cdot g^{-1}$ (omitting oxides). In addition, we have added molar element/calcium ratios to this table.

Referee comment: (10) I do not think your results allow any conclusions on whether higher Sr levels in water have or have not affected shell growth rate. If growth conditions remained invariant (aside from changing Sr levels), shells should have grown much more homogeneously. But in fact, there is a significant slowdown from LE1 over NE1, LE2 to NE2 suggesting that growth conditions deteriorated through time (Table 2).

Answer: We meant to articulate here that, while there is clearly a number of factors affecting shell growth in aquaculture, incorporation of Sr into the shell aragonite does not significantly affect growth rates in our

experiment. This is evident from Figure 6C, which compares Sr-labelled and unlabelled growth increments. This figure shows clearly that all data lie within the standard deviation of the average and differences are insignificant, however we have changed Table 2 values to daily growth values (as suggested further down by this reviewer) and believe this makes our point more clear.

Minor comments:

Referee comment: Please check orthography in entire ms. I am not familiar with the Australian English, and whether this represents a mix of American English (e.g., analyze, labelling, meter) and British English (analyse, labelling, metre).

Answer: We edited all the text (manuscript and supplement) to British English as outlined in the journal's author guidelines.

Referee comment: Consistent use of hyphenation is required in entire ms: crossed-lamellar, crossacicular, 3 mm-thick, high-resolution, crossed-lamellar, crossed-acicular, organic-rich etc. need a hyphen

Answer: Agreed and edited accordingly.

Referee comment: Headings: Consistently capitalize heading or use sentence case.

Answer: Agreed to use only sentence case.

Referee comment: No colon at the end of headings! E.g., P8L21: "The inner crossed[-]acicular [shell] layer:", P9L1, etc.

Answer: Agreed and edited accordingly.

Referee comment: P1L16, "aragonite crystals": As you noticed in the following sentence, "the smallest mineral units are nanogranules" which are enveloped by proteinaceous materials. I suggest to employ the term "mesocrystals", because the definition of an abiogenic aragonite crystal does not include nanocomposites consisting of aragonite and organic material.

Answer: Unfortunately, the referee's definition of the term 'mesocrystal' is not correct. Correctly, the term 'mesocrystal' refers to hybrid inorganic-organic nano-blocks that are aggregated to a crystal which exhibits the X-ray properties of a single crystal at the mesoscale (Cölfen and Mann, 2003). Or, as most recently defined by Bergström et al. (2015): **"**a nanostructured material with a defined long-range order on the atomic scale, which can be inferred from the existence of an essentially sharp wide-angle diffraction pattern (with sharp Bragg peaks) together with clear evidence that the material consists of individual nanoparticle building units**"**. Whether, or not some, or even all nanogranules are mesocrystals cannot be established here and is beyond the scope of the ms.

References for this answer:

Bergström, L., Sturm, E. V., Salazar-Alvarez, G., & Cölfen, H. (2015). Mesocrystals in biominerals and colloidal arrays. Accounts of chemical research, 48(5), 1391-1402

Cölfen, H., & Mann, S. (2003). Higher-order organization by mesoscale self-assembly and transformation of hybrid nanostructures. Angewandte Chemie International Edition, 42(21), 2350-2365.

Referee comment: P1L19, replace "shells" by 'shell portions' or 'ultrastructures'. There are no bivalves consisting entirely of nacre. I assume you intended to say that different ultrastructures contain different amounts of organics.

Answer: Agreed and replaced with "ultrastructures".

Referee comment: P1L19/20: I do not understand this sentence. Growth rates = growth patterns? Outer structure = outer shell layer. Prisms can be correlated to growth rates? Do you mean that each 3rd order prism forms in one day? Moreover, you did not mention anywhere in the text sub-daily growth patterns.

Answer: The timing of formation or the 3rd order prisms is mentioned in the text at P12L29: "while nanometre-sized third-order prisms form within hours (Fig. S6)." We have edited this sentence for clarity.

Referee comment: P1L20, "outer structure": You used the term "structure" in two different ways: as a synonym for "ultrastructure" and "shell layer" (e.g., P6L32). Be consistent. Do not use "structure", but one of the other terms above. Check and change throughout ms.

Answer: we agree and have replaced "structure" with either "ultrastructure" or "shell layer" (depending on the context) throughout the ms and supplement.

Referee comment: P1L23, "physiological processes during calcification have no lag": Rephrase, this is hard to understand. Shells do not just consist of CaCO3, but also organics which need to be fabricated, and the building blocks for these substances derive from ingested food. Digestion of food and fabrication of organic molecules that end up in the shell need time. There is hence a lag between ingestion of food and shell production. Or what do you mean with "physiological processes . . . have no lag".

Answer: We have edited this for clarity and down-toned the timing as we agree with this reviewer that there is most likely 'some' lag, reflecting 'some time' but that this lag is not significant enough to be quantified with our methods (see also comment to P13L29 below).

Referee comment: P1L23, "calcification" is the wrong term here (and used improperly in many other studies). Calcification rate includes density and is not synonymous to growth rate! Calcification rate = amount CaCO3 precipitated per time interval per area. Replace all instances with 'shell growth rate'.

Answer: In our study we were following the terminology as defined in Gillikin et al. (2005): "Considering that we discuss our results in the context of calcification processes, the distinction between growth rate and calcification rate should be made. In this study, the term growth rate is defined as the dorso-ventral linear extension of the shell per unit time (or growth increment per time)". "Calcification rate" and "crystal growth rate" are often used synonymously in sclerochronology to refer to the narrow growth increments and architectural arrangements at higher magnification of shell layers that are angled to the macroscopic dorso-ventral linear shell extension. However, "crystal growth rate" is in fact incorrect as "crystal" does not cater to the mesocrystalline nature of the material that is initially formed as ACC. Therefore, we use "local growth rate" to describe growth rates at higher resolution within different layers of the shell that are measured parallel to e.g. the long axis of first order prisms and that can be at angles with the macroscopic dorso-ventral linear shell extension. We have edited the corresponding paragraph in the manuscript and have replaced "calcification rate" with "local growth rate" all throughout the ms and supplement.

Reference for this answer:

Gillikin, D. P., Lorrain, A., Navez, J., Taylor, J. W., André, L., Keppens, E., ... & Dehairs, F. (2005). Strong biological controls on Sr/Ca ratios in aragonitic marine bivalve shells. Geochemistry, Geophysics, Geosystems, 6(5).

Referee comment: P1L25, "Sr-conditions": no hyphen; 'Sr level' or 'Sr concentration' sounds better

Answer: Agreed and edited accordingly.

Referee comment: P1L26, "Sr-enrichment": no hyphen

Answer: "Sr-enrichment factors" requires a hyphen. According to the Oxford Dictionary, a hyphen is required to link two words that function together as an adjective and that are placed before the noun they're referring to, hence, no change here.

Referee comment: P1L26, ”Sr-enrichment factors for labelled and ambient conditions”: This remains insufficiently explained and is oddly phrased. Do you mean artificially elevated Sr levels vs. normal marine Sr levels? Give actual numbers! What do you mean with "identical enrichment factors": Sr levels in shell increase proportionately to that in the water (i.e., 18 times)? As far as I can tell from Table 1, this does not apply to both shell layers (and ultrastructures).

Answer: As we have replaced the ‘enrichment factors’ with ‘distribution coefficient’ (Sr/Ca-shell)/(Sr/Ca-seawater) as suggested by reviewer 2 this sentence had to be edited anyway to reflect the new data. Also, we have followed this referee’s advice to give actual numbers.

Referee comment: P1L31, “aragonite or calcite”: replace “or” by ‘and/or’. Note there are species with different CaCO3 polymorphs in the outer and inner shell layers. Further note that some species also come with vaterite,

Answer: Agreed and edited as suggested.

Referee comment: P2L3: delete “recent and fossil”, superfluous

Answer: Agreed and edited as suggested.

Referee comment: P2L4+5: None of these papers used trace elements of shells as environmental proxies. Replace by suitable citations: (a) temperature: Klein et al. (1996a), Wanamaker et al (2008), Schöne et al. (2011), Zhao et al. (2017a). (b) salinity: Klein et al. (1996b). (c) pH: Zhao et al. (2017c)

Answer: We replaced the references with the suggested ones.

Referee comment: P2L12: substitute “shell” with ‘trace and minor elements in shells’

Answer: Agreed and edited as suggested.

Referee comment: P2L14: substitute “but” with ‘and’

Answer: was replaced with “however”.

Referee comment: P2L14: Firstly, always say ‘ultrastructure’, not “structure”, because at other places you use "structure" as a synonym for shell layer. Secondly, this statement needs a reference.

Answer: References are already given in the text (line 15) we replaced “structure” with “ultrastructure” were appropriate throughout ms and supplement.

Referee comment: P2L15-16: Delete sentence starting with “Apart. . .”. Then start next sentence with “Apart from those,”

Answer: No change

Referee comment: P2L17: replace “which are found” by ‘which occur’

Answer: edited as suggested.

Referee comment: P2L21: The homogeneous ultrastructure forms an own category and is not a subgroup of the crossed-acicular category (compare Marin et al. 2012)

Answer: We understand that there are different schools of thought. In the current version of our ms we have followed Shimamoto et al. 1986: “(…) homogeneous structure in the present study is used in broader sense

including crossed acicular and/or fine complex crossed lamellar structure of Carter (1980) (…)". Indeed, Marin et al 2012 state that "[crossed structures] represent a diversified group comprising the crossed-lamellar, complex crossed-lamellar, crossed acicular microstructures, found in most of the heterodont bivalves and in several gastropods". We have acknowledged both schools of thought in the revised version of the manuscript.

Referee comment: P2L21: "venerid" must not be italicized

Answer: edited as suggested.

Referee comment: P2L22: "Shimamoto, 1986" is outdated (?), check most recent revision of ultrastructures by Carter JG et al. (2012)

Answer: We checked Carter et al. (2012) and found that Shimamoto 1986 is not outdated in this aspect.

Referee comment: P2L33: replace "between umbo and ventral margin" by 'parallel to the main growth axis' or 'parallel to the umbo-ventral margin axis'

Answer: edited as suggested.

Referee comment: P3L5-6: "Growth lines. . ." show/refer to figure

Answer: We have added a reference.

Referee comment: P3L16: Two main clauses combined by conjunction require comma; check and correct throughout ms: ', and'

Answer: edited as suggested.

Referee comment: P3L17: Specimens: Much more information needed here: sediment type, tidal height, intertidal zone(?), how many specimens collected/prepared/used for which analytical technique, when collected. Table would be best. Part of this information is relevant for the temporal alignment of the shell growth patterns.

Answer: Referee has later (below) accepted our reasoning for the time gauge. We added the requested details to the corresponding paragraph.

Referee comment: P3L17: replace "live-collected" by 'collected alive'

Answer: edited as suggested.

Referee comment: P3L20: use 'x' as mathematical operator (consistently throughout ms)

Answer: edited as suggested.

Referee comment: P3L24-26: Has the element composition of the food been measured as well? How do you know that all Sr and Ca comes from the water? Has always the same amount of food being offered? When were they fed, during simulated day or nighttime?

Answer: We did not measure the Ca and Sr content of the diet. Food was added in the morning and we observed that the water had cleared up by the end of the day (after ca. 6 hours). This indicates an extended time of filter feeding (food uptake). If significant Sr and Ca were derived from the diet we would expect concentration differences (visible in maps) in unlabelled areas between shell portions formed during day and night. This was not observed.

Referee comment: P3L29-30: An "event" is a very short-term incident. This sentence should be rephrased, e.g., "exposure to background conditions, i.e., normal marine Sr levels".

Answer: rephrased as suggested. “Event” was chosen as it indeed refers to very short periods in accordance to what the reviewer says.

Referee comment: P4L7: P400-P2000

Answer: edited as suggested.

Referee comment: P4L12: thickness of gold-coating?

Answer: we added the thickness of the coating (15 nm) in the ms.

Referee comment: P4L21: 20,000x

Answer: edited as suggested.

Referee comment: P5L9: replace “was used” by “were used”

Answer: edited as suggested.

Referee comment: P5L21: µm2 (superscript)

Answer: edited as suggested.

Referee comment: P5L27 “The inner and outer layer of a *K. rhytiphora* shell were separated with a DREMEL tool and mechanically cleaned.” Be more specific here: Have you obtained powdered material or fractions of the two portions of the outer shell layer? How have you managed exactly to separate them?

Answer: We have clarified this in the revised version of the ms

Referee comment: P6L3: Actually wrong. You have only studied the outer shell layer, which consists of two portions with different ultrastructure, an outer and inner portion, respectively (oOSL, iOSL)!

Answer: We have replaced “inner layer” and “outer layer” with the nomenclature suggested by this reviewer throughout the ms and supplement.

Referee comment: P6L8: Rephrase (and italicize genus and species names): ‘The outer shell layer of studied *K. rhytiphora* specimens is ... near the ventral margin’

Answer: edited as suggested.

Referee comment: P6L10: “in agreement with previous studies**. . .**” This phrasing means that the other species studied by Carré and Soldati and colleagues lived in Australian waters. Rephrase.

Answer: edited to clarify that these are literature examples from the southern hemisphere but not from Australia.

Referee comment: P6L11: “growth periods”: delete “periods”

Answer: edited as suggested.

Referee comment: P6L13: “troughs” Odd phrasing. Something like this is better: ‘Cyclic changes in greyscale near the ventral margin correlate strongly with tidal cycles, i.e., light grey and dark grey portion fall together with full and new moon cycles, respectively. The main problem is that you do not provide any evidence for the timing of shell growth! Where is the evidence that the dark and light portions really have formed during new and full moon? This is an interpretation at most, and as such belong to the Discussion section (where you need to refer to previous studies of intertidal bivalves which found narrower increments and thicker growth lines formed during spring tides, and these portions then appear darker than shell portions formed during neap tides when viewed at lower magnification and under reflected light. More suitable Refs: Evans 1972, Schöne 2008, Hallmann et al. 2009)

Answer: We have moved these paragraphs to the discussion and have edited the text as suggested.

Referee comment: P6L16-25 also needs to be moved to Discussion. Only keep descriptive part here. You have no evidence that these grey bands formed on a circalunidian basis, but you can certainly interpret them as such based on previous work.

Answer: Moved as suggested.

Referee comment: Timing of shell growth: You later noticed that you observed 6 lines in portions formed in tanks during 6 days suggesting that at least these growth patterns are circadian. However, you have no evidence that the same applies to shell portions formed in nature. Given that the specimens lived in the intertidal (please provide details on tidal regime: diurnal or semidiurnal, tidal range etc.), it is reasonable to assume that they have formed circalunidian growth patterns. Here, please stick to descriptions, not interpretation.

Answer: Agreed – we revised this part and added that the shell areas formed in the natural environment perhaps follow circalunidian growth patterns.

Referee comment: P6L25: ‘in two other specimens’, not “on two other specimens”

Answer: edited as suggested.

Referee comment: Section 3.2: Title is more suitable for Discussion. – This section should be expanded as it is an essential component of the ms and forms the basis for your hypothesis on element incorporation. Describe Table 1 in much more detail. Report molar ratios as well. Compute and tell reader by how much the Sr levels increased in the shell when exposed to 18 times higher Sr levels in water. This will then show that the Sr levels in oOSL increased by 18 to 20 times, whereas the iOSL only by ca. 14 times. This needs to be discussed later.

Answer: The content of Section 3.2 “Validation of Sr incorporation” is a result and is thus indeed suitable for this section (no change). We now provide molar ratios in Table 2 and discuss these now is this section as well. We have also added the differences between labelled and unlabelled shell as well as the amount that Sr in the shell increases during labelling conditions.

Referee comment: P7L2: “. . .were identical within uncertainty”: i.e., they have remained invariant, stayed the same? I suggest you rephrase this to avoid confusion.

Answer: This is geochemically the correct terminology and means within *analytical* uncertainty.

Referee comment: Title Section 3.3: Section heading should inform about content of section, not which method has been used.

Answer: This section contains the Raman spectroscopy results and is, as such, correctly titled.

Referee comment: P7L31: “This species develops annual growth checks” On what evidence is this statement based? How did you analyze when the shell portions formed? Likely correct, but pure speculation... or is there previous work on this species?

Answer: Referee has below accepted our reasoning for the time gauge. No change necessary.

Referee comment: Section 3.4.3: Interesting information, but what is the purpose of having this measured and reported?

Answer: The amounts and composition of the organic moiety are not well known, particularly for non-nacreous shells. We are presenting new results here with the purpose of closing this knowledge gap. We note that the referee finds these results interesting.

Referee comment: P9L10: crystallographically

Answer: “crystallographic preferred orientation (CPO)” is the correct name of this type of data. No change.

Referee comment: P9 “Calcification Rates” includes density, not synonymous to growth rate! Calcification rate = amount CaCO3 precipitated per time interval per area; this is not what you mean.

Answer: see our answer above.

Referee comment: P9L28-29: “Due to the geometry of first order prisms without- and inward bending in cross-sections,. . .” No sentence

Answer: This sentence has been edited for grammar and clarity.

Referee comment: P10L2: Provide image showing where you determined increment widths, or even better trace two growth lines to show that growth in oOSL is faster than in iOSL due to shell geometry.

Answer: These images are already in the supplement.

Referee comment: P10L4-5: quite complicated phrasing: absolute growth rates vary among specimens

Answer: edited as suggested.

Referee comment: P10L5: grew, on average, 5.6... same for the other "on average": separate by comma and place before number

Answer: edited as suggested.

Referee comment: P10L12: “Also, rates tend to decrease effectively with increasing distance to the ventral margins (Fig. 4A).”: Unclear what you mean and purpose of mentioning this. You need to trace fortnights in Figure 4A to support your statement.

Answer: We have edited this part for clarity.

Referee comment: “bivalve species”: you listed genera not species rephrase: ... structure of other bivalves, e.g., Pinna..., the aragonitic...

Answer: edited as suggested.

Referee comment: P10L23, P11L5, P11L23: “In *K. rhytiphora* the first order prisms” comma after species name

Answer: changed as suggested.

Referee comment: P11L10: Equally-sized (adverbial usage)

Answer: changed as suggested.

Referee comment: P11L30: Since you did not capitalize "aragonite", you should also use lower case here (except for the acronym/abbreviated form). Besides that, you used lower case in the Abstract.

Answer: changed as suggested.

Referee comment: P12L30: replace “the outside of their shells” by ‘outer shell surface (Fig. 1), and’

Answer: changed as suggested.

Referee comment: P13L1: “growth time”: Firstly, you have no evidence that these growth checks formed annually. Secondly, no bivalve grows 365 days. Note also that such ornamentation patterns do not agree with growth patterns in other species, and likely this is a coincident and only true for shell portions near the ventral margin in the studied specimens. Rephrase.

Answer: Referee comment below retracts this one – hence no change. However, we seized this opportunity to emphasize that we are aware that no bivalve grows 365 days with the same rate but that this was a reasonable estimate that yielded a result in the correct dimension.

Referee comment: P13L12-13: Perfect! This is your time gauge. It verifies the circa daily nature of these growth features and could further be used to support your hypothesis of fortnightly growth bundles appearing as greyscale changes.

Answer: Thank you we have added a sentence suggesting the use of the increments to support our hypothesis of fortnightly growth bundles.

Referee comment: P13L14-15: replace “higher” with ‘faster’, “short” with ‘narrow’, “longer” with ‘broader’

Answer: changed as suggested.

Referee comment: P13L15: “day”: An interesting question that you need to discuss is that these are probably circadian (24h) periods entrained by the 12/12 light/dark cycle experimental conditions. The adjustment interval was probably long enough that the natural, tide-entrained shell formation cyclicality (resulting in circalunidian, 24.8h, periods) vanished. Under natural conditions though, you would need to have circatidal (12.4h) and circalunidian increments, because otherwise your interpretation of the other 48 or 50 dark cycles representing fortnight periods would not hold true.

Answer: We agree and have added this to the discussion of our data in the revised version of the ms.

Referee comment: P13L22: “We suggest a diel physiologically controlled variation of calcification” Not sure exactly what you mean. Circadian clock controlling growth/calcification rate? This has been reported previously elsewhere.

Answer: This part has been rewritten for clarity.

Referee comment: P13L29 “have no lag”? Well, this depends on the temporal scale you are looking at. Where is the evidence that there was no gradual increase in shell Sr levels during the course of minutes or so? Diffusion of Sr through the mantle epithelium takes at least some time.

Answer: See answer above – we edited this sentence for better temporal accuracy.

Referee comment: P13P29“physiological processes involving Sr incorporation”, rephrase: ‘physiological processes controlling Sr incorporation’

Answer: changed as suggested.

Referee comment: P13L30-31: I do not think that the implications provided are supporting an ACC mediated growth of shell in bivalves.

Answer: We rephrased this sentence accordingly.

Referee comment: P13L33-34: “A fundamental observation of this study is that the calcification front runs evenly across all structural units and architectural orders of the shell independently of the current growth rate. This” But this is known and no a new finding of this study!

Answer: We disagree. This was not known for compound composite prismatic and crossed-acicular shells and is an entirely new finding (we emphasised this aspect now more clearly in the revised version of the ms). We note the lack of literature evidence for the referee’s statement here.

Referee comment: P14L1: “show the labels to cut across the different architectural building blocks”: could also occur if extrapallial space is gel-filled or epithelial cells are in direct contact with shell

Answer: Agreed.

Referee comment: P14L2 “where the label would rather follow a zig-zag trend between fully labelled and unlabelled units” Impossible to understand what you intend to say here. Rephrase please. Do you mean that the growth front is uncoupled from the ultrastructures? This is known as well: In freshwater bivalves the large prisms continue to grow over many years and daily growth lines cross them perpendicularly (studies by Dunca, Mutvei etc.).

Answer: This part of the text has been clarified as we do not refer to the uncoupling of the ultrastructure. We disagree that this was already known. This was not known for compound composite prismatic and crossed-acicular shells.

Referee comment: P14L2-4: “This is clearly visible from the sharply defined change between labelled and unlabelled shell areas (Fig. 4B and D), as well as from the cyclic variations in short-term growth rates (discussed above). Our” Likewise hard to understand

Answer: has been revised.

Referee comment: P14L10 “active selective transport consuming Ca2+-ATPase enzymes”: transport consumes energy which is provided by ATP, and the enzyme that accomplishes the transportation is the Ca ATPase. Rephrase.

Answer: This part of the ms was omitted as we agreed on shortening this chapter.

Referee comment: P14L14-15 “We observed virtually identical enrichment factors for Ca and Sr (CaShell/CaSeawater and SrShell/SrSeawater) in labelled and ambient conditions (Table 3).”: Interesting point

of view! But this does not mean anything else than Sr/Ca shell increases proportionately to that of Sr/Ca seawater, and this has already been shown by Zhao et al. (2017), which you did not cite.

Answer: This section has been extensively rewritten according to insightful comments from reviewer 2 and the citation has been incorporated.

Referee comment: P14L15: "Sr-ion transport is independent from. . . " if so, the energy demand of the bivalve increases in order to keep the Sr out of the shell. Do you see a decrease in growth rate during Sr enrichment as opposed to 'normal' Sr levels in water?

Answer: This section was deleted.

Referee comment: P14L16-17: "Sr ion would be at the expense of a Ca ion": Not really clear what you mean; Since this is the essence of your paper, you need to describe this more clearly and convincingly. Why exactly can transport mechanism 1 not be true?

Answer: This section was cut upon revision.

Referee comment: P14L17: Replace "Sr-enrichment" by 'shell Sr concentrations'

Answer: changed as suggested.

Referee comment: P14L18: Ca/Sr: please also or only report Sr/Ca

Answer: We now use Sr/Ca ratios in the ms.

Referee comment: P14L19-20: Replace "Hence, the strong enrichment of Ca from seawater to shell" by 'strong enrichment of Ca in shell'

Answer: changed as suggested.

Referee comment: P14L25: "Ca to be transported as ACC-nanogranules to the calcification front (Loste et al., 2004; Addadi et al., 2006; Jacob et al., 2011; Zhang and Xu, 2013)." Check if all cited studied were using bivalves (not gastropods or other taxa), and which ultrastructures were analzed, report this here.

Answer: The point is here that ACC-nanogranules have been observed across ALL TAXA to be part of a common principle of biomineralization. We would be happy to refer the referee to review studies who do exactly what is suggested here, but which is beyond the scope of our study.

Referee comment: Section 4.5: Here you discuss more (and different stuff) than what the heading implies.

Answer: We disagree. All aspects and 'stuff' discussed here belong under this heading.

Referee comment: P15L12: italicize genus and species names

Answer: edited as suggested.

Referee comment: P15L14-15: "a systematic change in growth increments during Sr-enriched periods": Do you mean 'growth increment widths'? You need to highlight here again that food levels and other extrinsic factors that could potentially have affected growth rate remained unchanged during the experiment, and you would have expected invariant increment widths if Sr had no effect on growth rate... see comment further above on relationship between growth rate and Sr exclusion from shell

Answer: We have revised this part of the manuscript (yes we meant widths) and have added the information suggested by this reviewer.

Referee comment: P15L18: Replace “calcification” by ‘growth rate’

Answer: Replaced with “growth”.

Referee comment: P15L23-24: “Reduced growth rates in aquaculture conditions cannot be explained by ontogenetic trends alone but result from missing tidal cycles.” Sorry, but this is pure speculation and likely wrong. Much more likely is that you did not provide proper food and the animals did not really ’like’ the tank conditions.

Answer: It is well known that shallow water depths lead to reduced growth rates in intertidal bivalves and, hence, the aquaculture experiments (in which tides are difficult to produce) can be understood to have similar but prolonged effects comparable the low water levels in nature. We have added a citation and edited this sentence for clarity. Also the possibility of a switch from circalunidian to lunar days has been now mentioned and the sentence was toned down to show that we speculate this to be true. The reviewer’s suggestion that we haven’t provided “proper food” is completely groundless as we have purchased special diet that is distributed as one of the most high quality shell fish diets commercially available and that has been used in other studies and commercial aquacultures. Also, although growth rates were downregulated compared to nature they were stable within the experimental period as shown in this study (e.g. Table 2).

Referee comment: P15L30: ‘nanometer’?

Answer: British English, no change.

Referee comment: More comments in pdf with annotated figures and tables.

Answer see below.

Reviewer Comments from the Supplementary Information:

Referee comment: [To Fig. 1] I recommend removal of boxes around letters A, B, C...

Answer: We thank the referee for this suggestion. No change.

Referee comment: [To Fig. 1] FYI: The inner shell layer is formed inside the brown areas, whereas the brown section and portions outside thereof largely belong to the iOSL; the oOSL is likely not seen in this image.

Answer: Agreed as already clarified above, shell layers have been renamed.

Referee comment: [To Fig. 1] The pallial line is the small indentation ca. 1.5 cm away from the ventral margin on the inner shell surface. The pallial line strikes out again at the cardinal tooth (hinge; likewise a small kink developed). The inner shell layer is formed inside the portion delimited by the pallial line 'strikeouts'.

Answer: This is correct.

Referee comment: [To Fig. 1] Outer (A) and inner shell surface (B)...

Answer: edited as suggested.

Referee comment: [To Fig. 1] Denote: Arrows cannot be summers!

Answer: edited as suggested.

Referee comment: [To Fig. 1] Low or high values? dark or light grey?

Answer: clarified.

Referee comment: [To Fig. 1] Temporal alignment is purely speculative. Though I believe it is correct, you did not provide any convincing support this.

Answer: See referee comment above where they backtrack on this comment

Referee comment: [To Fig. 2] Captions should explain things. You fail to say what the pink and blue actually means: Sr enrichment in shell during immserion in Sr-enriched (give molar value) tank water and Sr shell levels during times of normal marine Sr conditions of 8.9 mmol/mol.

Answer: Agreed and clarified.

Referee comment: [To Fig. 2] Indicate DOG.

Answer: Edited as suggested.

Referee comment: [To Fig. 2] That are the inner and outer portions of the OUTER SHELL LAYER; B is not the inner shell layer!

Answer: Agreed and edited accordingly.

Referee comment: [To Fig. 2] This does not look polished, but etched.

Answer: This is a polished surface that received a final physical and chemical polishing step as explained in our methods section.

Referee comment: [To Fig. 2] You need to provide a schematic of the shell to show where exactly the images in Figures 2-5 were taken (hinge or ventral margin, where in the ventral margin?). As outlined below you only sampled the inner and outer portions of the outer shell layer, but not actually the inner shell layer.

Answer: In our first caption we state “All cross-sections in this study are prepared as radial sections along the maximum growth axis unless otherwise specified.”

Referee comment: [To Fig. 3] Denote DOG

Answer: Edited as suggested. We have added and/or edited all DOG errors in the ms and supplement as well to make it easier to distinguish between the overall growth direction of a shell and local growth directions as visualised by the label to make it less confusing for the reader.

Referee comment: [To Fig. 4] That's incorrect! You are still in the outer shell layer here. These are just two different portions of the outer shell layer. The inner shell layer is way back (below in this image) and starts where the myostracum intersects with the inner shell surface (= aka pallial line) and then ends somewhere at the hinge portion. Shell material is added laminarily along the entire inner shell surface beyong the pallial line and results in thickening of ontogenetically younger shell portions (near the umbo and hinge). The inner portion of the outer shell layer actually does the as the outer portion: contributes to size increase of the entire shell, but in addtion also contributes to thickening. I recommend to look at the Figure in Schöne (2013) for morphological details of a veneroid.

Answer: Already addressed above.

Referee comment: [To Fig. 5] I am lost here. Is this image mirrored and upside down? Can you just present it in the same way as Figure 4? And please describe here again which portion on the two sides of the dotted line is the inner (left of line?) and outer portion of the outer shell layer (right of line).

Answer: We have clarified the orientation of the map by adding a schematic of the shell tip to all EBSD maps in the ms and the supplement (as well as in some other figures to maintain clarity. We chose to present other EBSD maps in ms and supplement that we think are easier for the reader to understand. We have simplified the figures also by reducing the number of white arrows that indicate the overall shell growth direction to one as is common practice in other publication and use the pole figures and appearance of the Sr-label in the underlying BSE images to point out the local growth directions in the corresponding EBSD maps.

Referee comment: [To Fig. 6] agree with what? each other? Rephrase. Within each shell layer, growth rates are unaffected by exposure to higher Sr content in water. How have you actually tested this mathematically? Student t-test? Normal distibution test done?

Answer: The information that the four different increments in 6C are within errors is based on their positions of the diagram. We have rewritten this part of the caption to make it more accessible to the reader.

Referee comment: Table 1: without considering Ca... 18-20x oOSL, 13-14x iOSL, Why different? Why does only Sr level in oOSL change proportinately to Sr increase in water?

Answer: Firstly it is a general observation that values are higher for oOSL compared to iOSL as we state in the ms. It could be speculated that this is caused by the different overall growth rates between the two shell layers combined with the curvature of the shell.

Referee comment: Table 2: I do not understand "or". Which of the data in this column are 12d and 6d? For direct comparison of data, provide daily growth rates for all data.

Answer: The referee may have missed the explanation already provided (coded by italicised and normal text). We have now used a clearer coding (bold and normal). Daily growth are now provided as suggested.

Referee #2:

We thank this referee for their constructive comments, which will provided a helpful basis for the revision of our ms.

We appreciate that the referee feels that the way of presenting our large dataset is adequate. The referee noted that the ms is more on the descriptive side, and this is indeed a main in our work as this shell architectural type has never been studied at the micro to nano scale before. We see the work presented in this ms as a baseline for further work carried out on this type of shell architecture in the future, which necessarily needs to build on a detailed description.

In the following we are listing the referee's comments followed by our answer.

Referee comment: Description and interpretation of the data which related to crystallography and biomineralization seems to be OK, however, discussion about elemental transportation was based on very weak evidence thus problematic. Especially, the evidences the authors based on is (1) fluctuation of gray contrast observed at the growth portion during the Sr-enriched labelling experiments obtained by BSE image, even though BSE contrast is unreliable method for quantifying Sr concentration, and (2) similar enrichment factor (Shell/Seawater ratios) in labelled and non-labelled conditions in both ultrastructural layers aquired by EPMA analysis, while the way for presentation of this enrichment factor is not adequate for discussing the element transport. Because most of the discussion regarding biomineralization is good quality, and because the length of the MS is already enough, so I recommend to simply delete the contents related to element transportation.

Answer: We agree that the discussion about elemental transportation is a more speculative part of the manuscript and has been rewritten considerably. We also agree that BSE imaging per se is an unreliable method of quantification. This is exactly the reason why we went to great length to calibrate the grey scale of the BSE imaging by combining it with quantitative electron microprobe measurements using Wavelength

Dispersive Spectrometry (WDS) with the same instrument and in the same session as carrying out the BSE imaging. Such calibration enables direct comparison of the grey scales in the BSE images with the quantitative data using WDS in the Electron Microprobe. Further down in the text, the referee agrees with us on this point. We have added a sentence to the Results that explains this to the readers.

Referee comment: I would like to also suggest to add a new schematic drawing for summarizing the biomineralization and shell formation mechanisms obtained by this study. SEM and EBSD pictures are of course very nice, but they are sometimes too complicated for readers. A simplified drawing will be very helpful for readers to grasp the main conclusion of this MS.

Answer: We have added a schematic to the revised version of the ms as well as a new supplementary figure.

Referee comment: The authors not only examined the pulsed Sr-labelled portion of the shell, but also examined the shell comprehensively, so I recommend changing the title."

Answer: We believe the current title already reflects the 'comprehensive examination of the shell' as stated by the referee. The purpose of the label is to provide markers in time for the study of the entire shell. We will however reorganise and add the term 'shell' to the title to specify the aim of the study. We edited the title to be: '**Insights into architecture, growth dynamics, and biomineralization from pulsed Sr-labelled Katelysia rhytiphora shells (Mollusca, Bivalvia)**'.

Referee comment: P1, L24, L26-27, as mentioned above and below, the discussion of the element transportation is based on too weak evidence, so I recommend to deleting this part.

Answer: These sub structures were also observed in micro-Raman maps and reflect true changes in Sr concentration. We discuss this in more detail below (see referee comment P13, L13). However, we edited the abstract to make this point clearer to the reader.

Referee comment: P3, L31, More detailed information of labelled seawater circulation is necessary. Did the authors use a single batch of seawater, or prepare labelled seawater every time for changing the water? How robust was the stability of the Sr concentration? The seawater renewing was performed constantly or done at once? Because the authors did not provide seawater composition, the Sr fluctuation, if exist, is suspicious. Changes in Sr/Ca ratio in seawater can easily produce Sr/Ca fluctuation in the shell. This is very important and critical for the discussion for the elemental transport mechanism.

Answer: For labelling, seawater was enriched in Sr by adding 4.380 g Sr-hexachloride per 10 l of seawater and was freshly prepared each time the water had to be renewed. Renewing the water was done at the start and in the middle of each labelling period. As we used natural seawater from two large seawater storage tanks of 10,000 ltr capacity each and a high precision balance, precise to the third digit, we consider the Sr concentration data robust. We have added this to the materials and methods section.

Referee comment: P12, L1-17, I would suggest adding simulation data of Young's stiffness for two test cases, (1) Single aragonitic crystal, and (2) The same crystal arrangement, but have a random orientation of the crystals. Is it possible? The comparison between (1) and (2) will provide the contribution of complex 3D construction of multi-order unit of crystal arrangement, and that of between (2) and the results presented in the MS will provide a contribution of control of crystal orientation by bivalve, is this right? I am not familiar with the stiffness simulation, so I am not completely sure that this suggestion is pointing or not.

Answer: We have now included the Young's modulus for a single crystal. We have also included a reference to an earlier publication from our group that shows the Young's modulus for an aragonite single crystal as reference (Agbaje et al 2017). However, depicting a randomly oriented fabric in a pole figure means that the aragonite crystallographic axes will be randomly oriented. Therefore, the elastic properties of the crystal would be averaged and the fabric would be isotropic. A pole figure depicting an isotropic orientation would show an even distribution across the entire pole figure and would therefore be very uninformative to the reader. We added a sentence describing that a sample with random crystal orientation would lead to isotropic results.

References for this answer:

O.B.A. Agbaje, R. Wirth, L.F.G. Morales, K. Shirai, T. Watanabe, M. Kosnik, D.E. Jacob (2017). Architecture of crossed-lamellar bivalve shells: The Southern Giant Clam (*Tirana dears*, Roding, 1798). R. Soc. Open Sci. 4: 170622. http://dx.doi.org/10.1098/rsos.170622

Referee comment: P13, L13, the "bright grey areas" must not be caused "by variation in Sr concentration". It is OK to say that the contrast between labelled and non-labelled part is caused by the Sr concentration changes, because this is validated by Sr/Ca analysis by NanoSIMS and EPMA. However, the variation within the labelled portion was not be assured. Can you see this fluctuation also in Sr/Ca map? The contrast of BSE image is not only induced by Sr concentration but also by density (mass number) and topography. As the authors discussed, organic concentration can even change the contrast of BSE. If the authors want to discuss Sr concentration variation, they should be based on Sr analysis, not on BSE image. According to this, the evidence for the discussion at P13, L19-23 relies on very weak evidence. Additionally, the authors did not provide Sr and Ca composition of seawater, so it is difficult to exclude the possibility that this variation is attributed to the changes in seawater composition.

Answer: The resolution of the Sr/Ca maps obtained by NanoSIMS unfortunately do not allow to observe any variation at this spatial scale. As argued above, the Sr and Ca composition of the water, particularly during the labelling periods, is constant within analytical uncertainty and can thus be excluded as a source of grey scale variability in BSE. Neither did we observe growth irregularities (e.g. organic components) in these shell layers. Topography and edge effects would not result in such regular patterns of grey scales only within this very sharply defined layer as observed here. The fine grey banding, however, also shows up in the Raman maps (e.g. Figs.3, S2) and as Raman is not sensitive to electron density effects this would exclude these as a cause for the banding. Furthermore, deconvolution of the Raman signal is consistent with variation in Sr concentration as underlying cause for the grayscale banding observed in BSE, as increased Sr concentration in aragonite results in peak broadening (Fig. 3) and peak shift of the main carbonate band to lower wavenumbers (Fig. S2) (Alia et al., 1997, O'Donnell et al., 2008, Ruschel et al., 2012). This is direct evidence for the correlation of lighter grey scales in BSE with higher Sr concentrations in the aragonitic shell. Upon revision of the manuscript we will clarify this connection between BSE and Raman analysis more.

References for this answer:

Alia, J. M., Mera, Y. D. de, Edwards, H. G.M., Martín, P. G., and Andres, S. L.: FT-Raman and infrared spectroscopic study of aragonite-strontianite (CaxSr1− xCO3) solid solution, Spectrochimica Acta Part A: Molecular and Biomolecular Spectroscopy, 53, 2347–2362, 1997

O'Donnell, M. D., Fredholm, Y., Rouffignac, A. de, and Hill, R. G.: Structural analysis of a series of strontium-substituted apatites, Acta Biomaterialia, 4, 1455–1464, 2008.

Ruschel, K., Nasdala, L., Kronz, A., Hanchar, J. M., Többens, D. M., Škoda, R., Finger, F., and Möller, A.: A Raman spectroscopic study on the structural disorder of monazite–(Ce), Mineralogy and Petrology, 105, 41–55, 2012.

Referee comment: P14, L8-29, "4.4 Revisiting the Concept of Ion Transport Pathways". I recommend omitting this section because this section seems to be based on very weak evidence as mentioned above comments. In addition to the unreliability of BSE as Sr indicator, similar "enrichment factors for Ca and Sr (Ca-shell/Ca-seawater and Sr-shell/Sr-seawater" is not an appropriate parameter for discussing the elemental fractionation. This should be discussed by distribution coefficient (Sr/Ca-shell)/(Sr/Ca-seawater). Judging from the data in Table3, the data does not seem to satisfy enough robustness for discussing this topic. The authors also ignore fractionation between EPF (if exist) and carbonate. This can also produce low Sr/Ca ratio in the shell, without changing the EPF composition. No evidence was also presented for justifying the ACC formation obtained in this study. So, overall this section is not supported by the original data, thus should be omitted.

Answer: After reflecting on both reviewers' comments that this section is very speculative, we felt it was best to cut this section considerably and to focus only on discussing the distribution coefficients (Sr/Ca(shell)/Sr/Ca(seawater)) which are now presented in Table 3. Including possible fractionation by any potential EPF is extremely speculative and is therefore not warranted, however, we reflected the possibility of the potential fractionation by EPF (if existing) and toned down the assertive tone of this section.

Referee comment: P16, L1-6, Conclusion. The second conclusion is OK, but the first and third conclusions were not supported by the data presented in this MS, because of the reasons as mentioned above.

Answer: We have listed four conclusions and believe the referee is referring to conclusion two and four as being too speculative. We have re-written and modified these parts of the conclusion also with regards to referee 1's comments.

Referee comment: Minor comments: P2, L5-10, Organic macromolecules itself can also control trace element incorporation. See, Stephenson A. E., DeYoreo J. J., Wu L., Wu K. J., Hoyer J. and Dove P. M. (2008) Peptides enhance magnesium signature in calcite: insights into origins of vital effects. Science 322, 724– 727 Wang D. B., Wallace A. F., De Yoreo J. J. and Dove P. M. (2009) Carboxylated molecules regulate magnesium content of amorphous calcium carbonates during calcification. Proc. Natl. Acad. Sci. U.S.A. 106, 21511–21516.

Answer: Thank you for pointing out the omission of these important works that we have now cited in the new version of the ms.

Referee comment: P4, L14, Magnification is not necessary, because it will be ultimately depends on print or screen size.

Answer: Thank you, mention of the magnification factor has been omitted in the revised version.

Referee comment: P4, L26, What is “Phenom XL”? P5, L27, “DREMEL tool” is not adequate. Maybe you should provide information of producer company, or use general name?

Answer: Phenom XL is the product name of the SEM used in this study. Similarly, a DREMEL tool is the official name of this tool. The term SEM is mentioned in the same sentence with Phenom XL. We added the term ‘power tool’ after ‘DREMEL’ to make this clearer.

Insights into architecture, growth dynamics, and biomineralization from pulsed Sr-labelled *Katelysia rhytiphora* shells (Mollusca, Bivalvia)

Laura M. Otter[1], Oluwatoosin B. A. Agbaje[1], Matt R. Kilburn[2], Christoph Lenz[3,4], Hadrien Henry[1,3], Patrick Trimby[5], Peter Hoppe[6], Dorrit E. Jacob[1,3]

[1]Department of Earth & Planetary Science, Macquarie University, Sydney, NSW 2109, Australia
[2]Centre for Microscopy Characterisation and Analysis, University of Western Australia, Perth, WA 6009, Australia
[3]Australian Research Council Centre of Excellence for Core to Crust Fluid System (CCFS) / GEMOC
[4]Institute of Mineralogy and Crystallography, University of Vienna, Althanstr. 14, 1090 Vienna, Austria
[5]Oxford Instruments NanoAnalysis, High Wycombe, HP12 3SE, United Kingdom
[6]Particle Chemistry Department, Max Planck Institute for Chemistry, Hahn-Meitner-Weg 1, 55128 Mainz, Germany

Correspondence: Laura M. Otter (laura.otter@mq.edu.au)

Abstract. The intertidal bivalve *Katelysia rhytiphora*, endemic to south Australia and Tasmania, is used here for pulsed Sr-labelling experiments in aquaculture experiments to visualize shell growth at the micro- to nano-scale. The ventral margin area of the outer shell layer composed of (i) an outermost outer shell layer (oOSL) with compound composite prismatic architecture with three hierarchical orders of prisms and an (ii) innermost outer shell layer (iOSL) with crossed-acicular architecture consisting of intersecting lamellae bundles. All structural orders in both layers are enveloped by an organic sheath and the smallest mineralized units are nanogranules. Electron Backscatter Diffraction reveals a strong preferred orientation of the aragonite c-axes perpendicular to the growth layers, while the a- and b-axis are scattered within a plane normal to the local growth direction and >46 % twin grain boundaries are detected. The Young's modulus shows a girdle-like maximum of elastically stiffer orientations for the shell following the inner shell surface.

The bivalves were subjected for 6 days twice to seawater with an increased Sr concentration of 18x mean ocean water by dissolving 144 $\mu g \cdot g^{-1}$ Sr (159.88 Sr/Ca mmol/mol) in seawater. The pulse labelling intervals in the shell are 13x (oOSL) and 12x (iOSL) enriched in Sr relative to the Sr spiked seawater. All architectural units in the shell are transected by the Sr label, demonstrating shell growth to progress homogeneously instead of forming one individual architectural unit after the other. $D_{Sr/Ca}$ for labelled and unlabelled shell are similar to shell portions formed in the wild (0.12 to 0.15). All $D_{Sr/Ca}$ are lower than values for equilibrium partitioning of Sr in synthetic aragonite.

1 Introduction

The shells of bivalves are bio-composites with a complex, hierarchical 3D arrangement of crystalline calcium carbonate (aragonite and/or calcite), intimately conjoined by organic macromolecules that control nucleation and growth of the mineral entity across all length scales (Weiner and Traub, 1980; Rodriguez-Navarro et al., 2012; Simkiss, 1965; Addadi et al., 2006;

Cusack et al., 2008; Weiner et al., 1984). This arrangement significantly enhances the physical and mechanical properties of the shell and explains its high mechanical strength and fracture resistance (Currey and Kohn, 1976; Jackson et al., 1988; Kamat et al., 2000).

Trace elements incorporated in the carbonate phase of shells are used to monitor and reconstruct (paleo)environmental parameters, e.g. water salinity (Klein et al., 1996b), temperature (Zhao et al., 2017a; Klein et al., 1996a; Schöne et al., 2011), and pH (Zhao et al., 2017b). While the incorporation mechanisms of trace elements in mollusc shells are not yet fully understood, we do know that the incorporation of some trace elements, such as strontium, are influenced by local growth rates between different growth axes, shell curvature along the same axis, and physiological effects (Urey et al., 1951; Gillikin et al., 2005; Carré et al., 2005; Gillikin et al., 2008; Foster et al., 2009). Organic carboxyl-groups play a critical role for the incorporation of Mg into the shell (Stephenson et al., 2008; Wang et al., 2009; Shirai et al., 2012), but direct evidence for a similar role of organic molecules in the incorporations of other trace elements is lacking. Indeed, different trace elements (e.g. Mg, K, Ca, Sr) show distinctly different interaction with organic molecules and influence on mineral growth (Sand et al., 2017) showing that generalisation for the role of trace elements in biomineralisation are not straightforward.

A critical step forward in our understanding of how trace elements are incorporated into the growing biomineral is to gain better insight across all spatial scales into how different shell architectures are formed. Traditionally, studies on shell formation have been focusing on the nacreous ultrastructure (Checa et al., 2006; Nudelman, 2015), while more recently other ultrastructures, such as the crossed-lamellar architecture received increasing attention (Böhm et al., 2016; Almagro et al., 2016; Agbaje et al., 2017b). Here we present data and detailed characterization of two rarely investigated ultrastructures, namely the compound composite prismatic and the crossed-acicular ultrastructure, which are common to bivalves of the Veneridae family (Shimamoto, 1986).

We are using a combination of pulse Sr labelling aquaculture experiments and high-resolution microanalytical methods to gain insight into submicron architecture and growth dynamics in the two different portions of the outer shell layer. Pulse Sr labelling experiments have contributed significantly to our understanding of submicron scale growth mechanisms in marine calcifiers such as scleractinian corals, echinoderms and foraminifera (Shirai et al., 2012; Nehrke et al., 2013; Domart-Coulon et al., 2014; Gorzelak et al., 2014; Gutner-Hoch et al., 2016). Since pulse Sr labelling experiments provide time gauges for shell growth at high spatial resolution, this method enables study of time-resolved growth of individual submicron sized architectural units in the shell relative to local growth, which, due to the curvature of the shell, can vary by up to 90˚ in direction from the direction of dorso-ventral shell extension in bivalves.

2 Materials and methods

2.1 Aquaculture and pulsed Sr-labelling experiments

The “common cockle” or “ridged venus” *Katelysia rhytiphora* (Lamy, 1935) is a temperate, shallow burrowing, intertidal species that occurs along the shorelines of Tasmania and south-eastern to south-western Australia (Edgar, 2000). Some species

of the genus *Katelysia* are edible (*K. peronei, K. rhytiphora,* and *K. scalarina)* and have been a historical food source in Australia as seen by their occurrence in aboriginal shell middens (Cann et al., 1991). Today, *Katelysia* are produced in aquaculture (Nell et al., 1994), and shells in the wild are used to extract environmental parameters (Nell and Paterson, 1997). *K. rhytiphora* shells were collected alive at Port Lincoln, South Australia from fine- to medium-grained sand in the intertidal zone. Twenty-nine bivalves were placed in polyethylene boxes (20 x 40 x 10 cm, 7 bivalves per box) filled with sterilized beach sand and placed within 50 litre polyethylene tanks at the seawater facility at Macquarie University in September 2016. All tanks were connected to a recirculating system with filtered, sterilized natural seawater. Temperature and water chemistry, including salinity, pH matched ocean values. The setup in smaller sand-filled boxes enabled easy and quick transfer of the bivalves between the larger tanks, thus minimizing handling stress. Indeed, the bivalves were observed to continue filter-feeding while being transferred, which is a reliable sign for the absence of handling stress. Acclimatisation period was 3 weeks and experiments lasted 36 days. A 12h/12h day/night light cycle was maintained throughout the experiment and the water was homogenized using an air-stone. The bivalves were fed daily with a mix of microalgae "Shellfish Diet 1800" (Reed Mariculture Inc., USA) containing *Isochrysis sp., Pavlova sp., Tetraselmis sp., Chaetocerous calcitrans, Thalassiosira weissflogii,* and *Thalassiosira pseudonana*. After acclimatisation, bivalves were transferred twice for 6 days each to labelling seawater conditions at 18 x mean ocean water average of 144 $\mu g \cdot g^{-1}$ Sr (4.380 g $SrCl_2$ x $6H_2O$ in 10 l seawater). Between labelling events, bivalves spent 12 days at normal seawater conditions (ca. 8 $\mu g \cdot g^{-1}$ Sr). After the last labelling event, some bivalves were collected after 6 days at ambient conditions, while the remaining specimens were collected after 12 days. The pulsed Sr labelled periods are referred to as "labelling events", LE1 and LE2, whereas "normal events" NE1 and NE2 refer to background conditions, with ambient marine Sr levels. The water quality was maintained by fully renewing the spiked seawater every 48 hours with a freshly produced batch (using 4.380 g $SrCl_2$ x $6H_2O$ per 10 l seawater). Over the entire course of aquaculture an effort was made to keep the conditions (temperature, salinity, pH, lighting), including food availability, as stable as possible, so that Sr-concentration in the seawater was the only altered variable. After the experiments, bivalves were deep-frozen at -20 °C. After thawing and removing of soft tissues, shells were rinsed in deionized water and air-dried.

2.2 Sample preparation

Valves were cut along the maximum growth axis using an IsoMet low speed precision sectioning saw (Buehler, IL, USA). Left valves were mounted using EpoFix epoxy resin (Struers, Australia), while 3 mm-thick shell slabs from right valves were fixed on microscopy glass slides using metal bisphenol-A-epoxy resin (Permatex, Hartford, CT, USA). After curing at room temperature, sample surfaces were ground and polished using sandpaper (P400-P2000) as well as 3 and 1 µm diamond pastes. Left valves were further polished using a final chemical polishing step with a diluted suspension of colloidal silica (0.05 µm) for one minute on a neoprene polishing cloth to ensure optimum conditions for high-resolution analyses. Additional shell pieces were immersed in a solution of 1% wt./vol. ethylenediaminetetracetic acid disodium salt dihydrate (EDTA; Sigma-Aldrich), ultra-sonicated for 6 minutes, rinsed with Milli-Q water and air-dried. For SE-images un-etched broken shell pieces

and some etched with EDTA (1% wt./vol) were mounted on aluminium stubs using carbon glue, and gold-coated with a thickness of 15 nm.

2.3 Optical microscopy

A Leica M205C binocular stereomicroscope with reflective light was used to image shell slabs along the entire shell cross-section. Images were stitched and contrast improved in Adobe Photoshop CS5. To obtain greyscale line profiles, the image part containing the prismatic oOSL was cropped and further improved in contrast. Greyscale line profiles were acquired using ImageJ (Schindelin et al., 2015).

2.4 Electron probe micro analyser (EPMA), field emission gun scanning electron microscopy (FEG-SEM) and electron backscatter diffraction (EBSD)

Quantitative wavelength-dispersive X-ray spectroscopy (WDS) was carried out using a JEOL JXA 8200 electron probe micro analyser (EPMA) at the University of Mainz, Germany, with a defocused beam in rastering mode at 20,000 x magnification to obtain concentrations of Na, Mg, P, S, Cl, K, Ca, Mn, Fe, Sr, and Ba calibrated against a variety of minerals and synthetic reference materials (Table S1). Backscattered electron (BSE) images at lower magnification were acquired from carbon-coated polished cross-sections. Specimens were imaged with 15 kV acceleration voltage and 8 nA beam current at 11 mm working distance. Epoxy mounts and broken pieces of shells were imaged with field-emission gun scanning electron microscopes (FEG-SEM), namely a JEOL JSM- 7100F and a Phenom XL at Macquarie University (BSE images at 15 kV and 8 nA), and a ZEISS Leo 1530 at the Max Planck Institute for Chemistry, Germany, for secondary electron (SE) images (at 3 kV and 2 nA).

Electron backscatter diffraction (EBSD) data were acquired at Oxford Instruments NanoAnalysis, High Wycombe, United Kingdom, using a Hitachi SU70 FE-SEM equipped with an Oxford Instruments AZtec 3.4 EBSD-EDS system, with an X-Max 150 mm^2 EDS detector and a CMOS-based Symmetry EBSD detector. Three EBSD maps were collected along the axis of maximum growth in different regions of interest using 15 kV accelerating voltage, a beam current of 10 nA and a step size of 0.1 µm. The EBSD pattern resolution was 156 x 128 pixels at a collection rate of 195 patterns per second. Noise reduction was performed using the HKL software and datasets were processed using the MTex toolbox in Matlab (Bachmann et al., 2010; Mainprice et al., 2011) following the protocol in Henry et al. (2017). All EBSD data points were used for the calculation of the Young's modulus.

2.5 Micro-Raman spectroscopy

Raman spectra were recorded at room temperature using a Horiba Jobin Yvon LabRAM HR Evolution spectrometer coupled to an Olympus optical microscope with the laser beam path aligned through the microscope objective (quasi-backscattering configuration). A diode-pumped solid-state laser with 473 nm (~15 mW at sample surface) and a He-Ne laser with 633 nm (~10 mW at sample surface) excitation wavelength were used. Spectra recorded in the red spectral range (λ_{exc} = 633 nm) have

a spectral resolution of 0.8 cm^{-1} and a pixel resolution of 0.3 cm^{-1}; those recorded in the blue spectral range (λ_{exc} = 473 nm) have a spectral resolution of 1.6 cm^{-1} and 0.6 cm^{-1} pixel resolution using a grating with 1800 lines /mm.

Hyperspectral images were obtained using a software-controlled x-y table and a step width of 0.6 µm. All instrument set-up parameters and measurement conditions were kept constant during automated point-by-point spectra acquisition to guarantee subtle changes of Raman band parameters to be recorded reliably. Minute modification of Raman band parameters as obtained from hyperspectral mapping were interpreted only qualitatively. Data reduction included background subtraction and peak fitting using Lorentzian-Gaussian (pseudo-Voigt) function. All FWHM values were corrected for the instrumental apparatus function using the empirical correction published in Váczi (2014).

2.6 NanoSIMS analyses

Epoxy mounts were gold-coated prior to introduction into a new generation CAMECA NanoSIMS 50L ion probe equipped with a Hyperion RF plasma oxygen ion source, at the University of Western Australia. The primary oxygen ion beam was focused to a diameter of 100 nm and images were acquired from 100 × 100 μm^2 areas at a resolution of 1024 × 1024 pixels with a dwell time of 3.6 ms/pixel. ^{24}Mg, ^{40}Ca, and ^{88}Sr were measured on electron multipliers at a mass resolving power of 5000. The imaged areas were pre-sputtered at a slightly larger map area prior to acquisition. Images were processed using the OpenMIMS plugin for ImageJ/FIJI, where a correction for detector dead time was applied and the ratio of $^{88}Sr/^{40}Ca$ are expressed as a Hue-Saturation-Intensity (HSI) colour scale – min (blue) = 10, max (magenta) = 100).

2.7 Thermal gravimetric analysis (TGA)

Using a DREMEL power tool, fractions of both portions of the outer shell layer were obtained by removing the iOSL in one shell fragment and the oOSL in an other. Both samples were soaked in H_2O_2 (Merck KGaA, Darmstadt; Germany) for 1 hr at room temperature and washed with Milli-Q water. After air-drying, each sample was powdered using an agate mortar and pestle. Total amounts of organics were determined with a TGA 2050 thermogravimetric analyser (TA Instruments, USA). About 10 mg of powdered sample was measured (two replicates). The analysis was carried out under a nitrogen atmosphere, at a linear heating rate of 10°C/min, between 25–1000°C.

3 Results

3.1 Ultrastructure and shell growth

The outer surface of *K. rhytiphora* shells show prominent, concentric ridges (Fig. 1A) and a yellow and purple to brown pigmentation on the inside (Fig. 1B). The shell is fully aragonitic (Fig. S1) and our study focussed on the two architecturally different outer layers of the shell, to the outside of the pallial line. Underneath a very thin periostracum (see subchapter 3.4), the outermost outer shell layer (oOSL) consists of a compound composite prismatic architecture, while the innermost outer shell layer (iOSL) has a crossed-acicular ultrastructure. General thickening of the whole shell is achieved by the inner layer

beyond the pallial line (Fig. 1C). The oOSL of *K. rhytiphora* shells studied here is characterised by three dark bands near the ventral margin (Fig. 1C- E). A minor dark band at the very tip of the shell corresponds to growth in November when the bivalves were sacrificed (Fig. 1C-E).

The compound composite prismatic ultrastructure, which is considered to be one of the most complex shell architectures known represents an umbrella-term for a family of differently arranged hierarchical prismatic ultrastructures (Taylor, 1969; Popov, 1986; Shimamoto, 1986). First-order prisms in the oOSL have thicknesses between 10-30 µm and run parallel to the outer shell surface, with the long axis of the prisms oriented parallel to the main growth axis (Popov, 1986). These first-order units consist of 0.3 µm thick second-order prisms (Shimamoto, 1986) that protrude radially from the central axis of first-order prisms creating a feather-like appearance when viewed in cross-section (Taylor, 1969; Shimamoto, 1986). Each prism in both hierarchical orders is covered by a thin organic sheath (Taylor, 1969; Shimamoto, 1986). Taylor (1969) also observed smaller units within second-order prisms delineated by organic matrix and we refer to these units as third-order prisms here.

Two different schools of thought group the crossed-acicular ultrastructure with other structurally related architectures: Shimamoto (1986) classifies the crossed-acicular ultrastructure as a subtype of the homogeneous ultrastructure, while Marin et al. (2012) groups the crossed-lamellar, complex crossed-lamellar, and crossed-acicular ultrastructures together. The crossed-acicular ultrastructure has previously been comprehensively described for the marine gastropod *Cuvierina* (Carter, 1989) and consists of single lamellae that are arranged into bundles intersecting at angles of 120-150° with dipping angles of 30 to 40° relative to the inner shell surface (Carter, 1989).

3.2 Validation of Sr incorporation

Qualitative NanoSIMS mapping revealed two distinct bands of elevated Sr concentration in the oOSL at the ventral margin (Fig. 2A) as well as in the iOSL ca. 0.5 mm away from the ventral margin (Fig. 2B). Correlation of NanoSIMS maps with BSE images verify that light greyscales in BSE images are indeed caused by higher concentrations of Sr in the shell.

EPMA-based WDS analyses (Tables 1 and S2) show that Sr contents are generally higher in the oOSL than in the iOSL, averaging 19,500 $\mu g \cdot g^{-1}$ for the oOSL and 12,000 $\mu g \cdot g^{-1}$ for the iOSL (note that the value for iOSL is a minimum value as the analysed area slightly exceeds the label width). Strontium concentrations in growth regions formed before aquaculture (pre-aqua), during acclimatisation (pre-LE 1) and between labelling events (NE 1) are around 1,120 $\mu g \cdot g^{-1}$ for oOSL and again lower (1,010 $\mu g \cdot g^{-1}$) for the iOSL (Tables 1 and S2). Likewise, average molar ratios of Sr/Ca (mmol/mol) range from 1.32 (oOSL) and 1.18 (iOSL) in shell sections grown during ambient conditions in aquaculture to 14.55 (iOSL) and up to 23.60 (oOSL) in shell portions grown during pulse labelling. Hence, the increase of 18x mean ocean water concentrations (144 $\mu g \cdot g^{-1}$ Sr) in seawater resulted in a 13x increase in Sr in the oOSL (18,500 $\mu g \cdot g^{-1}$) in the labelled compared to the unlabelled conditions and in about 12x increase for the iOSL (>10,970 $\mu g \cdot g^{-1}$). Concentrations of other minor elements (Na, Mg, S, Cl) are generally lower in the iOSL and were identical within uncertainty between labelling and non-labelling experiments. Molar

ratios for Na/Ca and Mg/Ca range from 13.56 to 25.91 and from 0.76 to 1.05, respectively, and do not correlate with high Sr concentrations. Concentrations of Mn, Ba, P, K, and Fe in the shells are below detection limits.

3.3 Raman spectroscopy

Raman spot analyses in both studied shell layers show peak positions characteristic for aragonite (Fig. S1), namely a doublet at 701 and 705 cm^{-1} (ν_4, CO_3 in-plane bending), a peak at 1084.8 cm^{-1} (ν_1, CO_3 symmetric stretching), and several modes between 170 and 300 cm^{-1} that are due to rotations and translations of Ca^{2+} and CO_3^{2-} units (Urmos et al., 1991; Wehrmeister et al., 2010; Carteret et al., 2013). In addition, broad bands centred at 1134 and 1532 cm^{-1} represent C-C single bond (ν_2 stretching mode) and C=C double bond (ν_1 stretching mode) vibrations of polyene chains in organic pigments in the shell (Otter et al., 2017).

Micro-Raman hyperspectral mapping of the most intensive peak at 1084.8 cm^{-1} revealed that band widths (full-width at half-maximum, FWHM) differ between Sr labelled and unlabelled areas (Fig. 3). Two regions with systematic peak broadening in both ultrastructures correspond to the Sr labels seen as bands of light greyscale in BSE images and represent a change in concentration from 19,500 $\mu g \cdot g^{-1}$ Sr in labelled to 1,120 $\mu g \cdot g^{-1}$ in shell portions grown in ambient conditions. Although Sr concentrations in the seawater and duration of labelling conditions were identical for all labelling periods, the more recent outer label (LE 2) is narrower and brighter than in the earlier label (LE 1), reflecting different shell growth rates. Band width distribution shows distinct narrow increments within both labels.

Highest FWHM values within each labelled area are 2.2 and 2.7 cm^{-1} for the oOSL (Fig. 3A) and 1.8 and 2.4 cm^{-1} for the iOSL (Fig. 3B, Table S3), while FWHMs in unlabelled areas are less than 1.8 cm^{-1}. The ν_1 symmetric stretching band shows a shift in peak position to lower wavenumbers in areas of high Sr concentration (Fig. S2, Table S3). Note that FWHMs and peak positions do not vary among different architectural features in the unlabelled shell architecture, and hence, are not influenced by grain size effects.

3.4 Architecture of the shell layers

3.4.1. The compound composite prismatic architecture (oOSL)

As visible in radial sections of the oOSL (Fig. 4A) first-order prisms are oriented with their long sides parallel to the umbo-ventral margin axis and form a fan-like arrangement resulting in the ridged outer surface (Taylor, 1969; Popov, 1986; Shimamoto, 1986). First-order prisms originate and end at the organic-rich growth checks (Fig. 4A) and can reach sizes of >700 µm (projected 2D length) and widths of 17µm (aspect ratio of >40). Growth checks can be organic rich as observed here, or are fully mineralized with a different morphology, such as a thin layer of prisms (see below; Ropes et al., 1984). In contrast to studies that reported first-order prisms to exhibit square shapes in longitudinal cross-sections (e.g., Taylor, 1969), we observed irregular six-sided prism cross-sections in these *Katelysia* shells (Fig. S4). Measured widths of around 17 µm compare to literature values of around 10 µm for other venerid shells (Shimamoto, 1986). First-order prisms consist of second-order

prisms arranged radially around their central axis at an angle of 68° (Figs. 4B, S5), resulting in a feathery arrangement of second-order prisms in cross-sections (Popov, 1986; Shimamoto, 1986). Individual second-order prisms have projected lengths and widths of 3 ±0.3 µm and 0.3 ±0.06 µm (n=8), with an aspect ratio of 10. The widths are in accordance with values provided by Shimamoto (1986) for the shells of other venerid shells. Both first- and second-order prisms were found to be enveloped by organic sheaths as indicated by darker greyscales in the BSE images (Figs. 4A, B, S4) supporting literature findings for this ultrastructure (Shimamoto, 1986; Taylor, 1969).

Second-order prisms consist of third-order prisms (Fig. 4C), which are arranged with their long axes parallel to each other. They have lengths of 496 ±129 nm and widths of 67 ±16 nm (n=8, Fig. S6) with a lower aspect ratio of 8 compared to first- and second-order prism. Lastly, the smallest building blocks revealed by SEM images in etched shell samples are nano-granules with sizes in the range of 70 nm (Fig. 4E and F).

3.4.2. The crossed-acicular architecture (iOSL)

The acicular-prismatic boundary is marked by a ca. 30 µm wide transitional layer of granular texture comprising high numbers of short first-order prisms and spherulitic grains (Fig. S3). The growth check, which is organic rich in the oOSL, continues as a thin prismatic layer into the crossed-acicular ultrastructure of the iOSL (Fig.4A, green arrow). Bundles of cross-layered lamellae in the iOSL are enveloped by organic sheaths (dark grey, Figs. 4D, S7) and measure up to 1.4 x 0.8 x 0.2 µm (Fig. S8). Individual acicular lamellae are 1.8 ±0.4 µm long and 0.22 ±0.05 µm (n=19) wide with aspect ratios of about 8 (Figs. 4D, S7). The angle between acicular lamellae is 81 ±8° (n=6). Similarly to the oOSL, etching revealed a nano-granular texture in this layer (Fig. 4F).

3.4.3. Organic content

Thermal gravimetric analysis (TGA) was used to determine the total amount of organic macromolecules in the shell, which amounts to 1.42 ±0.03 wt.% and 2.19 ±0.04 wt.% for the iOSL and oOSL, respectively (Fig. S9). The organic phases are visible after etching the mineral phase and exhibit fibre- and sheet-like shapes (Fig. 4E, F).

3.5 Crystallographic preferred orientations

The ultrastructure of the aragonite grains in the oOSL and iOSL shell layers is shown in the orientation map in Fig. 5A. The map is colour-coded using an inverse pole figure colour scheme and shows the crystal direction in the orientation map facing the reader with blue, green, and red for the crystallographic a- [100], b- [010], and c-axis [001], respectively. Fig. 5A shows the feathery arrangement of the second-order prisms within the first-order prisms (outlined in green) as described above. The rims of the first-order prisms in the oOSL are well-resolved in the orientation map (Figs. 5, S10), while most of their cores remains dark and unindexed, indicative of poor or non-existent diffraction patterns as measured during the EBSD indexing cycle. We believe this effect is an artefact of sample polishing arising from preferential removal of the nearly vertically oriented

second-order prisms in these areas (Fig. S11). The alternative explanation, namely reduced crystallinity in these areas is highly unlikely as this would have been detected in Raman maps via significant band-width changes (Figs. 3, S2).

The iOSL with crossed-acicular architecture shows ca. 17 µm by ca. 10 µm large areas of lamellae, where the aragonite crystallographic axis are well co-orientated (Fig. 5A, outlined in yellow) and have high amounts of crystallographic twin boundaries (Figs. 5, S12).

Pole figures (Fig. 5B) show a strong preferred orientation of the aragonite c-axes perpendicular to the growth layers in the crossed-acicular architecture, while the crystallographic a and b axes are scattered on a plane normal to the local growth direction. The local growth direction in the crossed-acicular ultrastructure (green arrow in Fig. 5B) is perpendicular to the light grey Sr labels in the underlying BSE image and at this locality differs by ca. 90° from the general shell growth direction (white arrow). In comparison, the local growth direction of the compound composite prismatic layer (oOSL: purple arrow in Fig. 5B) has a smaller angle with the general shell growth direction. We identified a high abundance of twinning with 46% (oOSL) and 56% (iOSL) of the grains showing at least one twin (i.e. 63.8° ±5° rotation around the 001 axis).

3.6 Local growth rates

The pulsed Sr labels are easily visible in both the oOSL and the iOSL in BSE images as bands of bright greyscale (Fig. 4A). In general, greyscale values in BSE images cannot be relied on for trace element quantification. In this study, however, we have calibrated the BSE grey scale using quantitative WDS-based EPMA measurements in the same analytical session. Moreover, correlative mapping of the Sr distribution with NanoSIMS and micro-Raman spectroscopy (Figs. 2, 3, S2) clearly correlates the bright greyscales in the BSE images spatially with the Sr-labelled areas. Thus, in this study, greyscales in the BSE images reflect variations in Sr concentrations on the shells without any doubt.

Commonly, bivalve shell growth rates are reported as the macroscopic linear dorso-ventral shell extension ("general growth direction" in this study). Our high magnification images require us to take into account that local growth directions of the architectural units differ from the macroscopic linear dorso-ventral shell extension axis. Previously, these have been referred to as "crystal growth rate" (e.g., Gillikin et al., 2005; Carré et al., 2006). Instead, we use the term "local growth rate", because "crystal growth rate" does not reflect recent research that established the mesocrystalline nature of the material, initially formed as amorphous calcium carbonate.

Table 2 summarises the average local daily growth rates for all experiments (for detailed dataset see tables S4, S5). Length measurements were acquired in triplicate at five different locations on cross-sections along the maximum growth axis using the software ImageJ (Figs. S14, S15, Tables S4, S5). Although sizes and ages of the bivalve shells are similar, absolute local growth rates vary among specimens, especially for the oOSL (Fig. 6A, B). On a daily average within 6 days of pulsed Sr-labelling procedure, layer LE1 grew 0.93 ±0.15 µm (range: 0.37 – 2.22 µm), while layer LE2 grew 0.60 ±0.12 µm (range: 0.43 – 0.80 µm; Tables 2, S4). A 12-day ambient period (NE1) resulted in an average daily growth of 1.02 ±0.09 µm (range: 0.31 – 1.86 µm). The last 12-day ambient period (NE2) resulted in an average daily growth of 0.76 ± 0.08 µm (range: 0.47 – 1.41 µm). In comparison, the crossed-acicular ultrastructure (iOSL) grew only 0.88 ±0.10 µm (range: 0.58 – 1.17 µm) during

LE1 and 0.72 ±0.05 µm (0.62 – 0.92 µm) during LE2. Twelve days of ambient conditions (NE1) resulted in 0.75 ±0.04 µm (0.31 – 1.13 µm) daily average growth and for NE2 in 0.47 ±0.03 (0.43 –0.84). Based on average daily growth rates, oOSL grew 17 % faster than iOSL, which showed steadier growth (i.e. smaller standard deviations). Growth rates decrease with increasing distance to the ventral margin along iOSL (Fig. 4A). Individual Sr labels offer further detail and comprise several narrow increments of varying width and greyscale intensity in both ultrastructures (Figs. 4B, D). A systematic shift towards faster or slower local growth rates during Sr incubation was not observed (Fig. 6C).

4 Discussion

4.1 Multiscale architecture

Compared to simple prisms in the nacroprismatic bivalve ultrastructure the compound composite prismatic ultrastructure of *K. rhytiphora* is far more complex, containing three orders of prisms with sizes ranging from mm (first-order prisms) to nm (third-order prisms; Figs. 4A-C, S11). With respect to the number of hierarchically distinct units, the compound composite prismatic ultrastructure shares more similarity with the crossed-lamellar architecture than with the simple prism ultrastructure (Agbaje et al., 2017b). In *K. rhytiphora*, the first-order prisms run perpendicular to the growth checks and radially with respect to the radial cross-section (Fig. 4A) and comprise two orders of acicular prisms with high aspect ratios that are arranged feathery (radially in 3D around the central prism axis) in the case of second-order prisms and parallel in the case of third-order prisms (Fig. 4B, C).

Organic contents of both shell layers, namely 2.2 wt.% in the oOSL and 1.4 wt.% in the iOSL (Figs. 4E-F, S9), are intermediate between nacroprismatic shells (3-5 wt.% total organic content) and the highly mineralized crossed-lamellar shells with less than 1 wt.% organic content (Agbaje et al., 2017a).

Second-order prisms in the oOSL are co-oriented across their thin organic envelopes and, likewise, lamellae in the iOSL show co- orientation over 10 µm (Figs. 6A, S10). Co-orientation across the delineating organic sheath in the shell is a general observation for all bivalve shell architectures (e.g., Gilbert et al., 2008; Agbaje et al., 2017b) and is the result of the epitaxial growth mechanism via mineral bridges across the organic scaffolding (Checa et al., 2011). This model involving mineral bridges was developed for growth mechanisms in nacre, which has comparatively thick organic interlamellar sheets of ca. 30 nm and where 150-200nm sized mineral bridges are indeed visible (Checa et al., 2011; Nudelman, 2015). The organic sheaths in the *K. rhytiphora* shells are significantly thinner than the interlamellar membranes in nacre and mineral bridges across these would only require a few nanogranules of $CaCO_3$, the 30-50nm sized basic building blocks in bivalve shells (Wolf et al., 2016).

The crossed-acicular ultrastructure (iOSL) is built less complex than the prismatic ultrastructure (oOSL) and consists of only two architectural orders: (i) cross-layered individual lamellae of a few microns in length are angled at approx. 80° to each other and have dipping angles of <20° towards the inner shell surface, and (ii) cross-layered bundles of co-oriented lamellae at a higher hierarchical order (Fig. S8). Similar bundle-like arrangements of crossed-acicular lamellae were observed

by Carter (1989) in the marine gastropod *Cuvierina*, but these show larger angles to each other and smaller dipping angles than those observed in this study. In orientation maps for the iOSL (Figs. 5A, S12), some pseudo-prisms (Pérez-Huerta et al., 2014) can be identified (outlined in yellow) that consist of co-oriented lamellas.

A common structural motif of aragonitic bivalve shells is the high amount of crystallographic twinning. In *K. rhytiphora*, we observed 46 % (oOSL) and 56 % (iOSL) twin boundaries. Similar to amounts reported for crossed-lamellar (26%) and nacreous (20-65%) ultrastructures (Chateigner et al., 2000; Agbaje et al., 2017b). Aragonite twinning in bivalve shells encompasses all length scales including the nano-scale (Kobayashi and Akai, 1994) and values obtained by EBSD are minimum values as they are a function of the spatial resolution.

The smallest mineralized unit of both ultrastructures in the shells are granules with sizes of tens of nanometres (Fig. 4E). These granules are similar in size to the nano-granular texture observed in nacroprismatic and crossed-lamellar shell samples and have been found to be a common motif for bivalve shells (Jacob et al., 2008; Wolf et al., 2016; Agbaje et al., 2017b). Previous studies showed that these granules are often less well-crystallized or even amorphous and are enveloped by thin organic sheaths (Jacob et al., 2008; Wolf et al., 2012). They are most often the vestiges of a non-classical crystallization pathway via amorphous calcium carbonate ACC (de Yoreo et al., 2015).

4.2 Mechanical properties

The mechanical properties of shells i.e. stiffness, impact resistance, and toughness outcompete aragonite single crystals by several magnitudes (Jackson et al., 1988; Wang et al., 2001; Katti et al., 2006) Through evolutionary fine-tuning bivalve shells optimize their mechanical properties via their hierarchical organization, crystallographic twinning, nano-granularity, and the intimate intergrowth of mineral and organic phases at the nanoscale and aim at minimizing anisotropy in certain directions of the shell (Weiner et al., 2000). An important parameter to describe the stiffness of a material in response to stress and strain is the Young's modulus (Hashin, 1962). Young's moduli for *K. rhytiphora* shells, calculated from the EBSD dataset and the elastic constants of aragonite single crystals (Liu et al., 2005) yield a maximum of 139 GPa for the iOSL (Fig. 7A), 132 GPa for the oOSL (Fig. 7B), resulting in 135 GPa for both shell layers together (Fig. 7C). These values are in the range of those reported for crossed-lamellar (Agbaje et al., 2017b) and nacreous shells (Fitzer et al., 2015). The mechanical anisotropy can be defined as 200*(max-min)/(max+min) with max and min being the maximum and minimum values in GPa. For both layers, the mechanical anisotropy reaches 30%. The stereographic projection of the Young's modulus (Fig. 7A-C) reveals a girdle-like maximum of elastically stiffer orientations for the shell that differs significantly from aragonite single crystals (Fig. 7D), but is similar to results for other bivalve shells (Agbaje et al., 2017b). In reference to the shell morphology, this non-random arrangement of crystallographic orientations results in a quasi-isotropic plane of maximum fracture resistance parallel to the local growth lines (GL, Fig. 7A-C) and perpendicular to the local growth direction (and thus curvature) of the shell. Hence, the strongest, most fracture-resistant direction in the shell is parallel to its surface, thus maximising the shell's protective function.

4.3 Growth features and growth in the wild

K. rhytiphora shells form ornamental ridges on their outer shell surface (Fig. 1), and it is an interesting question how these ridges relate to shell growth. In the case of specimen K2-04 (Fig. 4), the ridge feature spans the area between the two most recent growth checks (Fig. 4A), suggesting a one year growth period for the ridge feature, which is also supported by estimating the growth period using growth rates for this specimen (2.2 µm/day using LE1). However, ridge features are not always associated with growth checks (Fig. 4A, purple arrow). Ridges are evenly distributed and similar in width (Fig. 1C), resulting in a decrease in the number of ridges per year with ontogenetic age of the shell. Similar to our findings for *K. rhytiphora* the surface spines of the gastropod *Strombus gigas* were found to be produced at different periods of time across different individuals, suggesting a genetic rather than an environmental control (Radermacher et al., 2009).

Looking at the formation of the ridge features in more detail, specimen K2-04 shows that the beginning of a new ridge as a fine protruding tip (Figs. 4A, S16), is associated with the highest local growth rates (2.2 µm/day using LE1, Table 2, Fig. S14). Evaluating this observation across all shells shows that at the same point in time, those shells with higher growth rates (e.g. 1.86, Table 2, Fig. S14) started producing their next ridge feature (Fig. S14D, E) while those shells with lower growth rates (e.g. 0.37, 0.46, Table 2, Fig. S14) lag behind (Fig. S14B, F). Supporting the delicate protruding tip of a new ridge by modulating growth rates could be a protective mechanism for this growth feature.

A major difference in the growth patterns between both layers of ultrastructures is that while the growth front in the iOSL is homogeneous and runs straight (Fig. 4D), the growth front in the oOSL is undulated (Fig. 4B and outlined in Fig S13). The centres of first-order prisms in the oOSL protrude compared to their rims (Fig S13) and the constant thickness of the Sr-labelled shell demonstrates that growth rates, measured perpendicular to the growth front, are homogeneous across this area. This undulation is not observed in other prismatic ultrastructures (simple prismatic ultrastructure: Dauphin et al., 2018) and the underlying reasons for this are yet unknown.

Total growth for oOSL and iOSL in aquaculture are on average 28.4 µm (oOSL) and 24.2 µm (iOSL) with daily growth rates of 0.85 ± 0.11 µm for oOSL and 0.73 ±0.07 µm for iOSL (Table 2). Consistent with the curved geometry of the shell and as previously documented (Carré et al., 2005; Foster et al., 2009), the oOSL in *K. rhytiphora* grows 17 % faster than iOSL (Table 2, Fig. 6), and growth rates for this layer are less variable than for the oOSL, both within individual specimens and across the population (Tables 2, S4, S5). While first-order prisms extend between two growth lines and are likely annual, second-order prisms (3 to 6 µm long, Fig. S5) and crossed-acicular lamellae (1.8 µm, Fig. S7) grow at rates of days in our aquaculture experiment, while nanometre-sized third-order prisms (Fig. S6) form within hours. Note however, that while growth rates for the architectural units relative to each other are valid, absolute growth rates in the wild are likely higher compared to aquaculture.

In fact, some insight into shell growth in the wild can be gained from shell portions predating the aquaculture experiments and are described here for the shell section depicted in Fig. 1, which is representative for three specimens in which these observations were made: Alternating light and dark bands seen in the shell cross-section (Fig. 1C-E) represent winter

(light bands) and summer (dark bands) shell growth. This is verified from the final dark band at the tip of the shell that corresponds to growth in late November when the bivalves were sacrificed. Cyclic changes in the greyscale line profile across these bands (Fig. 1C, D) correlate with tidal cycles: light grey and dark grey portions fall together with full and new moon cycles, respectively (Fig. 1D) and indicate that this shell section was deposited over the period two years. Intervals between grey-shaded areas in Fig. 1D correlate well with neap tides. This growth pattern is in accordance with findings that shell growth is strongly influenced by tidal cycles (Evans, 1972; Schöne, 2008; Hallmann et al., 2009), whereby neap tides result in light coloured increments that are generally wider than the dark increments (Rhoads and Lutz, 1980; Schöne et al., 2002; Carré et al., 2005; Carré et al., 2006). Hence, *K. rhytiphora* shells in the wild show a well-defined fortnightly shell increment resolution. Micro-growth bands at the outermost shell tip (Fig. 1D, red box) can be correlated with tides at the sampling locality at Port Lincoln, South Australia from mid-August to mid-September 2016 (Fig. 1E) and indicate that these micro-growth bands formed over this period in 2016 and prior to aquaculture (started mid-September 2016). From this time onward, the line profile ceases to correlate with tides (Fig. 1D, E blue band) and shell increments formed during aquaculture are very dark, reflecting lower than normal growth rates.

Analysis of the Sr labelled bands in the shell at high magnification by Backscatter Electron Microscopy allows further insight into growth conditions in aquaculture: Sr label LE1, for example, (Fig. 4B, oOSL) consists of pairs of bright, narrow and darker, wide increments (Fig. S17A). Identical patterns can be seen in the micro-Raman maps (Figs. 3, S2) and confirm that these variations in greyscale observed in BSE are caused by variable Sr concentrations in the labelled shell portion. A similar pattern is observed in the iOSL (Fig. S17B). It is noteworthy that the number of increment pairs in the label matches the number of days in Sr-enriched conditions (Fig. S17A, B) although the bivalves were maintained at constant conditions (including amount and timing of feeding) with Sr concentrations being the only varied parameter. This indicates that the acclimatisation period of three weeks at the start of the aquaculture experiments was enough for the bivalves to adjust from their circatidal and circalunidian cycles in the wild to the circadian cycle in aquaculture.

4.4 Implications for growth dynamics and biomineralization in pulse Sr labelled shells

Rather than gradual transitions in greyscale, the changeover between labelled and unlabelled areas in the shells is characterized by a ca. 500 nm narrow greyscale transition in the oOSL (ca. 150 nm in the iOSL), which is roughly equivalent to shell growth over 5 hours at the growth rates for this shell and this particular local growth rate (K2-04: 2.22 µm/day (oOSL) and 0.72 µm/day, Table 2). The activation volume of the incident electron beam, which could falsify the width estimate of the transition in greyscale is ca. 250 nm (Goldstein et al., 2017); Fig.17A, B), thus does not affect our estimate here. These short-term Sr-concentration changes in the shell thus mirror the immediate change in experimental conditions reasonably well, where seawater was replaced completely both at the start and the end of each Sr-enriched incubation and show that there is no significant lag between change in seawater Sr concentration and Sr incorporation in the shell. This suggests that in the biomineralization of this bivalve species there is no role for a significant ‘Sr-reservoir’, which would otherwise retain Sr-

concentrations different to the respective batch of seawater and cause gradual changes in greyscale in the BSE images of the shells over a wider shell portion.

One such biomineralization reservoir in bivalves is thought to reside in the space between the mantle epithelium and the growth front of the shell, namely the extrapallial space. The fluid in this space contains high concentrations of Ca^{2+}-binding proteins, important agents in biomineralization (Cusack et al., 2008; Rousseau et al., 2009). Our findings that the change in Sr-concentration in the shell closely mirrors the batch-changes of seawater suggest however, that the extrapallial fluid cannot be very voluminous, if it exists at all (Addadi et al., 2006; Marin et al., 2012). These results also demonstrate that changes in Sr concentrations (and, by inference also changes in concentrations of other trace elements) are recorded in the shell without significant temporal delay, which underscores the high suitability of bivalve shells as high-resolution archives of environmental change (Schöne et al., 2005).

An important finding of this study is that all hierarchical architectural units in both shell layers are transected by the Sr label (Fig. 4B, D, summarised in Fig. 8). Thus, rather than forming one individual architectural unit after the other, the growth front in the shell progresses homogeneously, transecting not only all mineral units, but also their individual organic envelopes. Naturally, and consistent with other pulse labelling studies on marine calcifiers the macroscopic morphology of the growth front follows the outside morphology of the skeleton. Nevertheless, at the micron to submicron scale, the homogeneous growth front observed here highlights a fundamental difference to growth processes in other calcifying organisms, where growth fronts are extremely heterogeneous in morphology and in growth rate (Gorzelak et al., 2014; Domart-Coulon et al., 2014). Our observation also potentially challenges the prevailing model for the formation of nacre by successive filling of pre-existing empty organic envelopes (Bevelander and Nakahara, 1969; Levi-Kalisman et al., 2001). Instead, our results for *K. rhytiphora* call for a more dynamic shell growth mechanism that allows for simultaneous formation of organic sheaths and mineral components, perhaps along the lines of models of calcification via directional solidification as recently proposed by Schoeppler et al. (2018).

4.5 Strontium/calcium ratios in the shell

The Sr/Ca ratio in bivalve shells has been used as a proxy for sea surface temperature (e.g., Dodd, 1965; Swan, 1956; Zhao et al., 2017a). However, a plethora of studies argues that Sr/Ca ratios in bivalve shells are mainly influenced by growth rate (e.g., Takesue and van Geen, 2004) and metabolic rate (Bailey and Lear, 2006; Foster et al., 2009; Gillikin et al., 2005; Purton et al., 1999) rather than by temperature. Distribution coefficients $D_{Sr/Ca}$ calculated as $(Sr/Ca_{unlabelled\ shell})/(Sr/Ca_{mean\ ocean\ water})$ for both shell layers in this study are very similar for labelled and ambient aquaculture conditions (0.14 and 0.15, Table 3) and are only slightly higher than those in the wild before aquaculture (0.13 for oOSL and 0.12 for iOSL). These $D_{Sr/Ca}$ values are in a similar range as aquaculture-derived $D_{Sr/Ca}$ for shells of the freshwater bivalve *Corbicula fluminea* (0.19 - 0.29, Zhao et al., 2017a), however these values, both for *K. rhytiphora* and *C. fluminea* are significantly smaller than $D_{Sr/Ca}$ for equilibrium incorporation of Sr/Ca in synthetic aragonite of 1.19 at 20 °C (Gaetani and Cohen, 2006). This discrepancy once again highlights the complexities involved in the interpretation of the chemical signatures in biominerals and their correct application

to arrive at accurate reconstructions of past environments. While the exact reasons for the large difference between synthetic and biomineralised aragonite are yet unknown, multi-step fractionation mechanisms connected with the step-wise nonclassical crystallization pathway (Jacob et al., 2017), which is the confirmed formation pathway for many calcifying organisms (de Yoreo et al., 2015) could play a major role.

4.6 Effects of aquaculture and pulsed Sr-labelling on growth and composition of the shells

Reduced growth rates are a common observation for bivalves held in aquaculture and *K. rhytiphora* in this study is no exception. A major contributing factor to reduced growth rates in aquaculture for intertidal bivalves such as *K. rhytiphora*, is the very different environment with respect to tidal cycles and lower water depths (e.g., Pannella and MacClintock, 1968). The strong influence of tides on shell growth for intertidal bivalves is well known (Rhoads and Lutz, 1980; Schöne et al., 2002; Carré et al., 2005; Carré et al., 2006), hence an aquaculture protocol that takes increased water pressures into account would be expected to enhance growth rates in future experiments.

The Micro-Raman maps demonstrate the influence of the incorporation of high Sr concentrations on the aragonite crystal structure: In the Sr- labels the $\nu_1[CO_3]$ ν_1 symmetric-stretching band-position is broadened by ca. 0.5 cm^{-1} (Fig. 3) and down shifted by ca. 0.5 cm^{-1} (Fig. S2, Table S3) compared to the areas formed at ambient conditions. This peak shift as well as the peak broadening results from changes in the interatomic distances in the aragonite crystal structure and slightly increase in structural disorder due to the incorporation of the larger Sr ion on nine-fold coordinated smaller Ca-sites (Alia et al., 1997). These effects on the Raman bands of the anionic complexes in minerals are typical when larger cations are substituted in the crystal lattice (Bischoff et al., 1985; O'Donnell et al., 2008; Ruschel et al., 2012).

Hence, while Raman spectra show that Sr-labelling has a measurable effect on the crystal structure of the aragonitic shell, this effect is minor, because (i) Sr substitution into the shell aragonite does not result in formation of a discrete $SrCO_3$ phase, which would have been detected as a band at 1073 cm^{-1} (Alia et al., 1997), and (2) analysis of the EBSD data (Figs. 6, S10, S12) does not show systematic deviations between the labelled and ambient areas in the shell. Furthermore, daily local growth rates of Sr-labelled and unlabelled areas, do not show systematic trends (Fig. 5C). Hence, while shell growth rates are downscaled during aquaculture, the multi-scale architecture of the shell down to the atom-level show no significant deviation from natural shells, indicating that the shell growth processes in aquaculture under the conditions chosen in this study are comparable to those in the wild.

Hence, pulsed Sr-labelling experiments offer the potential to study calcification processes down to the sub-micron range without apparent alteration of the growth processes and offer excellent analytical detectability for a wide range of micro-beam techniques. Pulse Sr-labelling is thus superior to experiments with fluorescent markers that are limited to the spatial resolution of light microscopy and have been shown to impact vitality and biomineralization processes in some calcifiers (Russell and Urbaniak, 2004; Thébault et al., 2006; Allison et al., 2011; Gorzelak et al., 2014).

5. Conclusion

Pulsed Sr-labelling experiments and correlated, in situ NanoSIMS and Raman mapping together with WDS spot analysis and FEG-SEM BSE imaging resolve local growth rates at the nanometre scale and show compelling potential to shed light on submicron growth mechanism in bivalve shells:

- All hierarchical architectural units and intercalated organic sheaths are transected by the Sr label and demonstrated bivalve shell growth to progress homogeneously instead of forming one individual architectural unit after the other.
- Sharp transitions between labelled and unlabelled shell areas indicate that physiological transport processes for Sr have no significant lag and suggest that the extrapallial fluid cannot be very voluminous.
- Both architectures have similar $D_{Sr/Ca}$ for labelled and unlabelled shells that agree well with those of shell formed in the wild and are all significantly below $D_{Sr/Ca}$ for equilibrium incorporation of Sr/Ca in synthetic aragonite.

Data availability

All data can be accessed by email request to the corresponding author.

Author contribution

LMO and DEJ designed and coordinated the study. LMO conducted aquaculture experiments, sample preparation, analyses. OBA, CL, and PH, participated in data collection. NanoSIMS and EBSD data were collected by MRK and PT, respectively. HH participated in EBSD data processing. All authors contributed to the manuscript and gave final approval for publication.

Conflict of interest

The authors declare that they have no conflict of interest.

Acknowledgements

We acknowledge Michael W. Förster, Antje Sorowka, Steve Craven, and Jacob Bynes for help and advice on sample preparation. We thank the Macquarie University Faculty of Science and Engineering Microscope Facility (MQFoSE MF) for access to its instrumentation and support from its staff members Sue Lindsay and Chao Shen. Jane Williamson and Josh Aldridge are thanked for access to and assistance at the Macquarie Seawater Facility. Wayne O'Connor (Port Stephens Fisheries Centre, NSW Department of Primary Industries) is thanked for insightful discussions on husbandry protocols. The authors received financial support through an Australian Government International Postgraduate Research Scholarship (IPRS) awarded to LMO, a Macquarie University Research Excellence Scholarship (iMQRES) awarded to OBA, and DEJ is supported

through an ARC Discovery Grant (DP160102081). C.L. gratefully acknowledges funding through the ARC Centre of Excellence CCFS at Macquarie University, Sydney and financial support by the Austrian Science Fund (FWF), through project J3662-N19.The authors acknowledge Microscopy Australia, the Science and Industry Endowment Fund, and the State Government of Western Australian for contributing to the Ion Probe Facility at the University of Western Australia. We are grateful to the handling editor, H. Kitazato, and 2 anonymous reviewers for their constructive comments.

Figures and figure captions

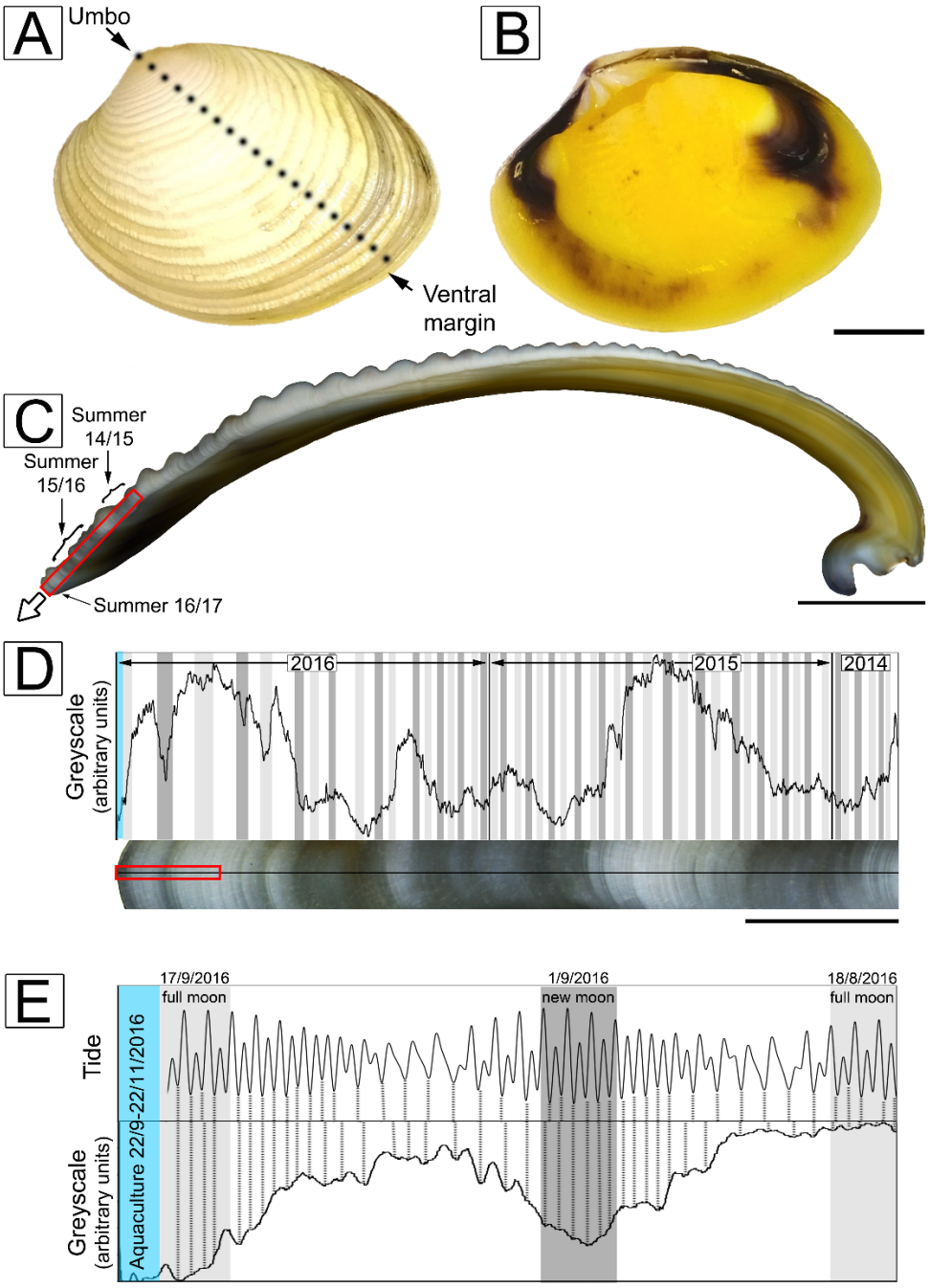

Figure 1: Outer (A) and inner shell surface (B) of an unlabelled *K. rhytiphora* shell. Dashed black line in (A) indicates where the shell was cut to produce the cross-section where a white arrow in (C) indicates the general growth direction of the shell. All cross-sections in this study are prepared as radial sections along the maximum growth axis unless otherwise specified. Dark bands (indicated by

arrows in C) result from growth during summer between lighter coloured winter periods and are magnified in D (red box in C) with a greyscale line profile. Darker greyscale intensities correlate with 48 out of 50 spring tides in two years from the collection site of the bivalves (full moon: light grey, new moon: dark grey) suggesting a fortnightly growth resolution in this shell area. Greyscale line profiles (E) of the area marked by the red box in D shows the most recent dark shell growth increment formed in the wild (mid-August to mid-September 2016). In this shell part, tides correlate with most shell increments (black dashed lines), while this correlation is lost after start of aquaculture (blue area). Blue area in D, E marks the aquaculture period with lower than normal growth rates. Scale bars are 10 mm (A-B), 5 mm (C), 1 mm (D), 0.1 mm (E).

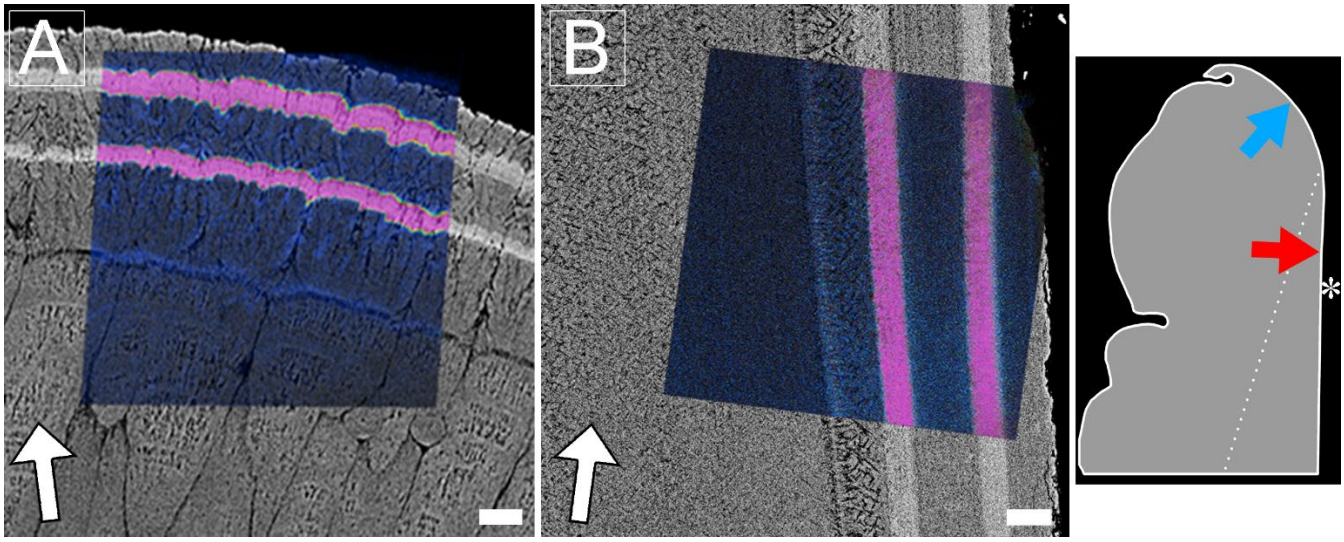

Figure 2: FEG-SEM BSE images showing polished cross-sections of the oOSL (A) and iOSL (B) of a Sr-labelled *K. rhytiphora* shell (specimen ID: K2-06) overlain with NanoSIMS $^{88}Sr/^{40}Ca$ maps. Shell layers grown in ambient seawater $^{88}Sr/^{40}Ca$ ratios are depicted in blue, while shell formed during Sr-enriched incubations are shown in pink. White arrows point towards the general growth direction of the shell, while the Sr-labelled shell layers from the underlying BSE image visualise the local growth directions for each ultrastructure. A schematic of the shell tip shows the exact location of the NanoSIMS maps with a blue and red arrow pointing towards the locations of the prismatic oOSL (a) and crossed-acicular iOSL (b) sampling location, respectively. Asterisk marks the inner shell surface. Scale bars are 10 µm.

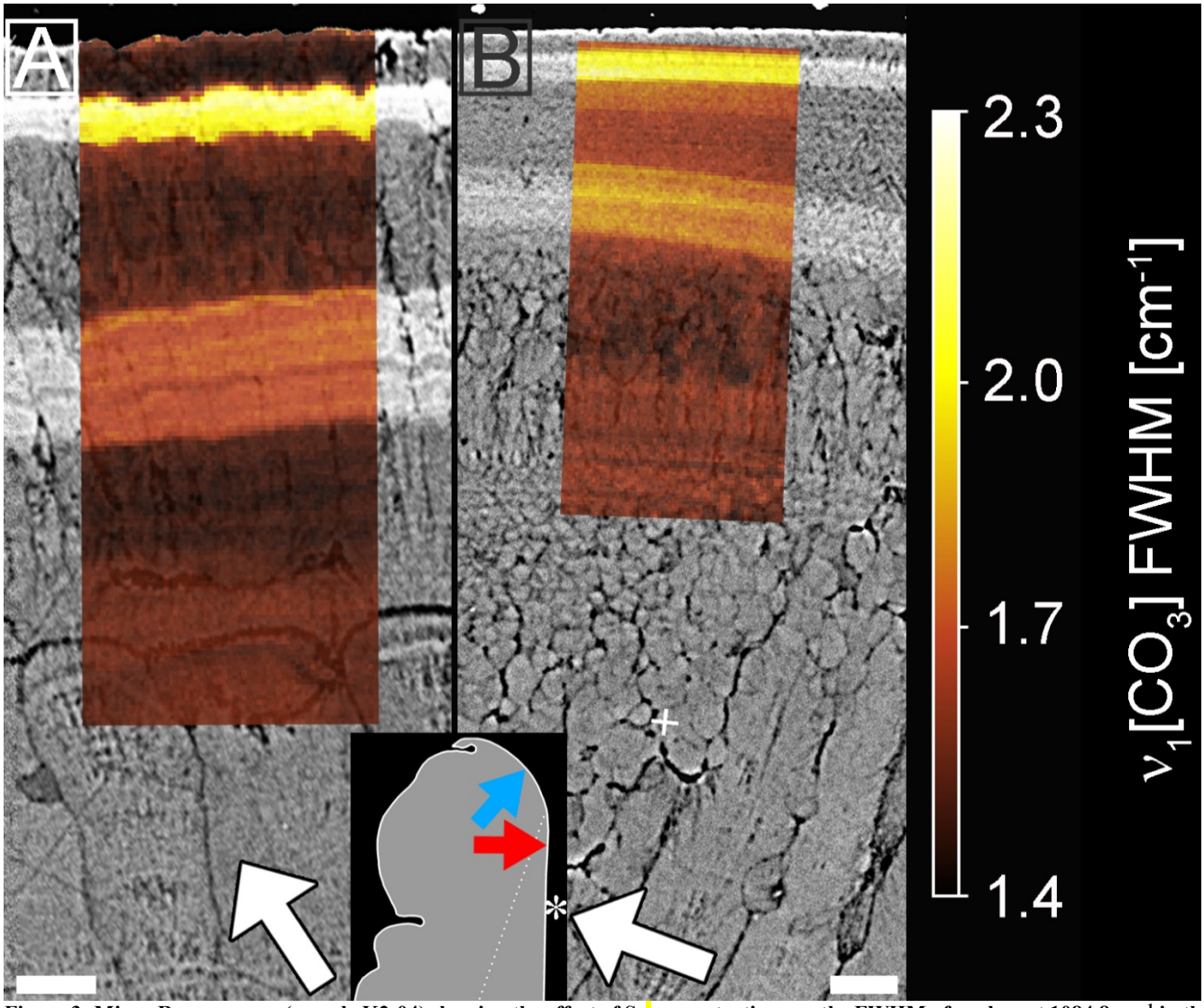

Figure 3: Micro-Raman maps (sample K2-04) showing the effect of Sr concentrations on the FWHM of peak ν_1 at 1084.8 cm^{-1} in the oOSL (A) and iOSL (B). Raman maps are overlain on BSE images. White arrows point towards the general growth direction of the shell, while the Sr-labelled shell layers from the underlying BSE image visualise the local growth directions for each ultrastructure. For Micro-Raman maps of peak shifts see Fig. S2. All values are bandwidth corrected after Váczi (2014). A schematic of the shell tip shows the exact location of the Raman maps with a blue and red arrow pointing towards the locations of the prismatic oOSL and crossed-acicular iOSL sampling location, respectively. Asterisk marks the inner shell surface. Scale bars are 10 µm.

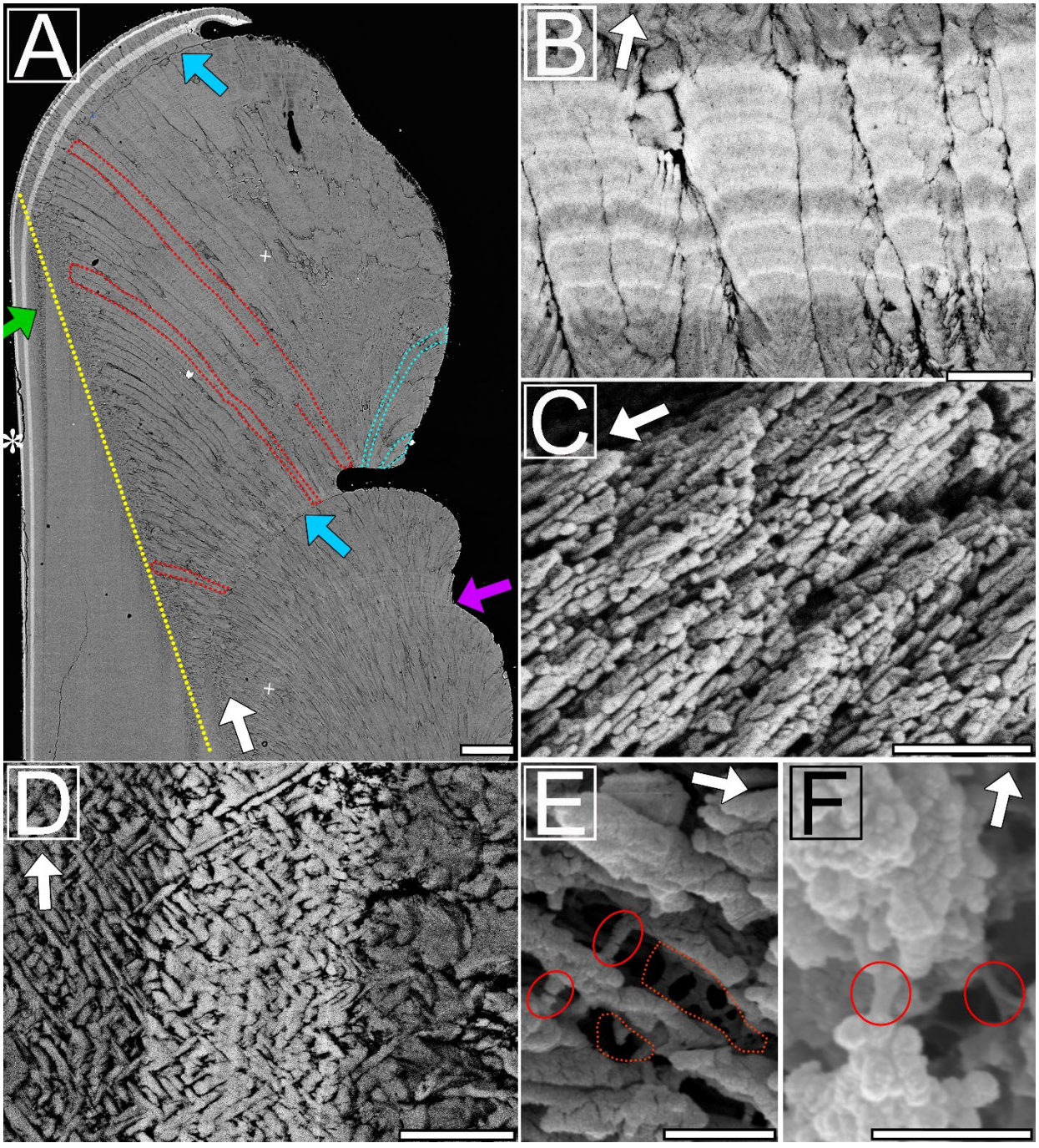

Figure 4: Electron images showing a cross-sections along the maximum growth axis of Sr-labelled *K. rhytiphora* shells: (A) BSE image shows the ventral margin of the shell. First-order prisms in the prismatic oOSL bend inwards (red outlined) reach lengths of up to 700 µm with widths of 17 µm. Outward bending prisms (blue outlined) form the ridged surface ornamentation of the shell.

Growth checks (blue arrows) are observed to occur directly at the end of ridge feature, while not all ridge features are concluded by growth checks (purple arrow). The yellow dashed line marks the boundary between iOSL and oOSL. Both Sr labels show bright greyscales and follow the growth front of the shell. In the iOSL, the growth check continues as a prismatic layer (green arrow). Strontium-labels within the oOSL (B) show first-order prisms to consist of radially arranged second-order prisms, which in turn consist of third-order prisms with their long axis parallel to each other, as seen in a broken piece of shell (C, SE-image). The iOSL has a crossed-acicular ultrastructure (D, BSE image) that is composed of needle-like lamellae intersecting at an angle of ca. 82°. Etched specimens (E, F: SE images) reveal the nano-granular texture of the mineral phase as well as organic compounds with fibre (red circles) and sheet-like structures (dashed red lines) in the prismatic (E) and crossed-acicular (F) layers. White arrows point towards the general growth direction of the shell, while the Sr-labelled shell layers in BSE images visualises the local growth directions for each ultrastructure. For more details see Fig. S3-S8. Scale bars: 100 µm (A), 5 µm (B and D), and 500 nm (C, E and F).

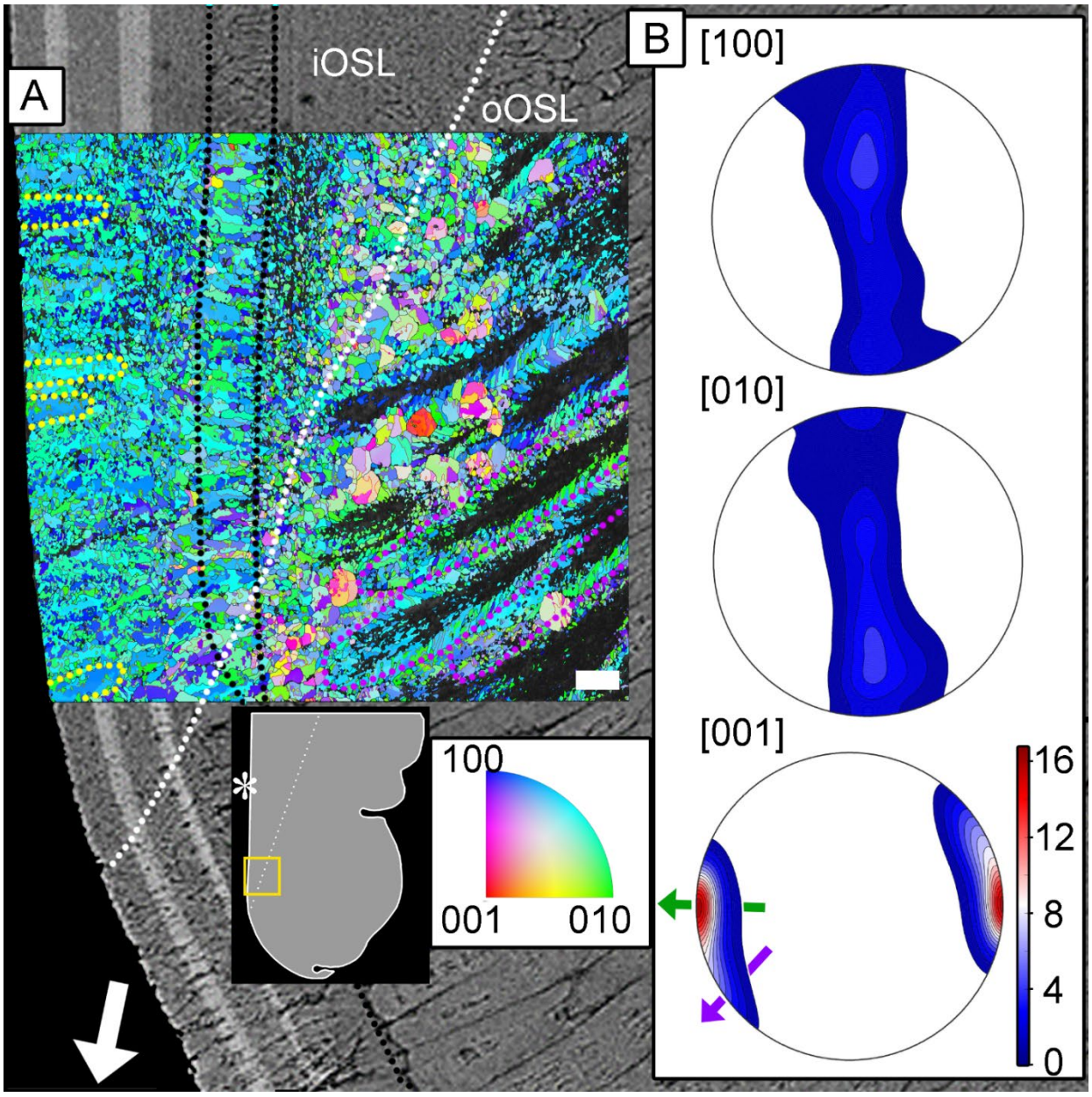

Figure 5: Orientation map for aragonite (A) of a pulsed Sr-labelled shell (specimen ID: K2-11) overlain on the BSE image of the same area. The dotted white line indicates the boundary between the crossed-acicular iOSL and prismatic oOSL shell layer portions. The organic growth check in the oOSL that continues as a prismatic layer in the iOSL is highlighted with black dotted lines. Blue, green, and red colours depict the crystallographic a- [100], b- [010], and c-axes [001] of aragonite, respectively. Twinned grain boundaries are presented in red. The map is color-coded to show the crystallographic orientation normal to the image plane. Predominantly green and blue colours in the map indicate that the a-[100] and b-[010] axes are randomly aligned mainly normal to the image plane. First-order prisms in the oOSL (some outlined in purple) have unindexed cores, and feathery arranged second-

order prisms are visible at their rims. Individual lamellae of the iOSL form co-oriented stacks up to 17 µm in size (circled in yellow). Pole figures (B) (lower hemisphere, equal area projection) show a strong clustering of the [001] axes for both layers. The local growth direction of the iOSL (green arrow), perpendicular to the light grey Sr-labelled layers in the underlying BSE image, differs by about 90° from the general growth direction (white arrow in (A)). The local growth direction of the oOSL (purple arrow) has a smaller angle with the general shell growth direction. The crystallographic a- and b-axes are randomly distributed in a plane normal to the local growth direction (i.e. parallel to the growth lines of the iOSL). Maximum density values of pole figures are colour-coded according to scale with the [001] axes achieving 16.8 times uniform. A schematic of the shell tip shows the location of the orientation map and the BSE image. Asterisk marks the inner shell surface. Scale bar is 10 µm.

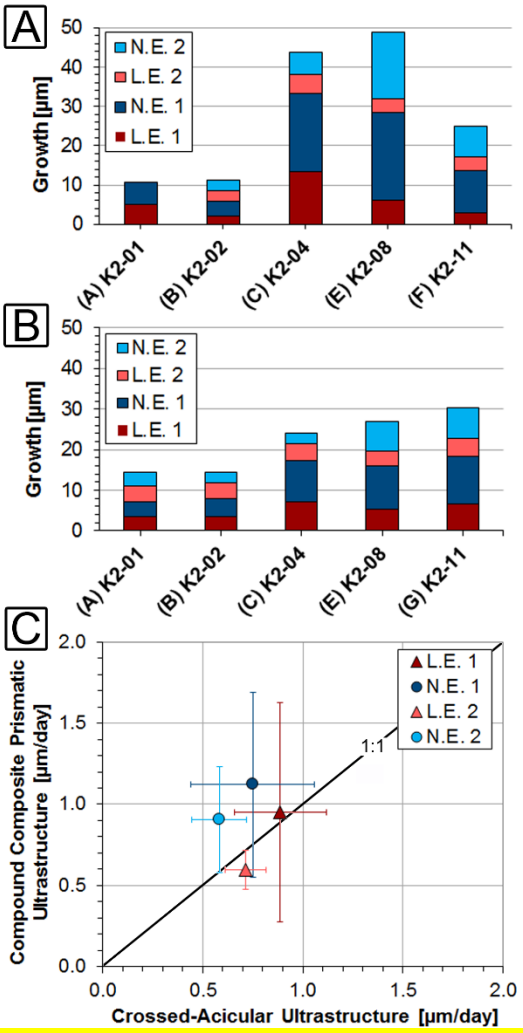

Figure: 6: Average growth of the compound composite prismatic (oOSL) layer (A) and crossed-acicular layer (iOSL) (B) (for values see Table 2). Distances were measured in triplicate at 5 different locations (Fig. S14, S15) along the axis of maximum growth using the software ImageJ. Local growth rates shown in (C) agree well within the first standard deviation between labelling and ambient conditions.

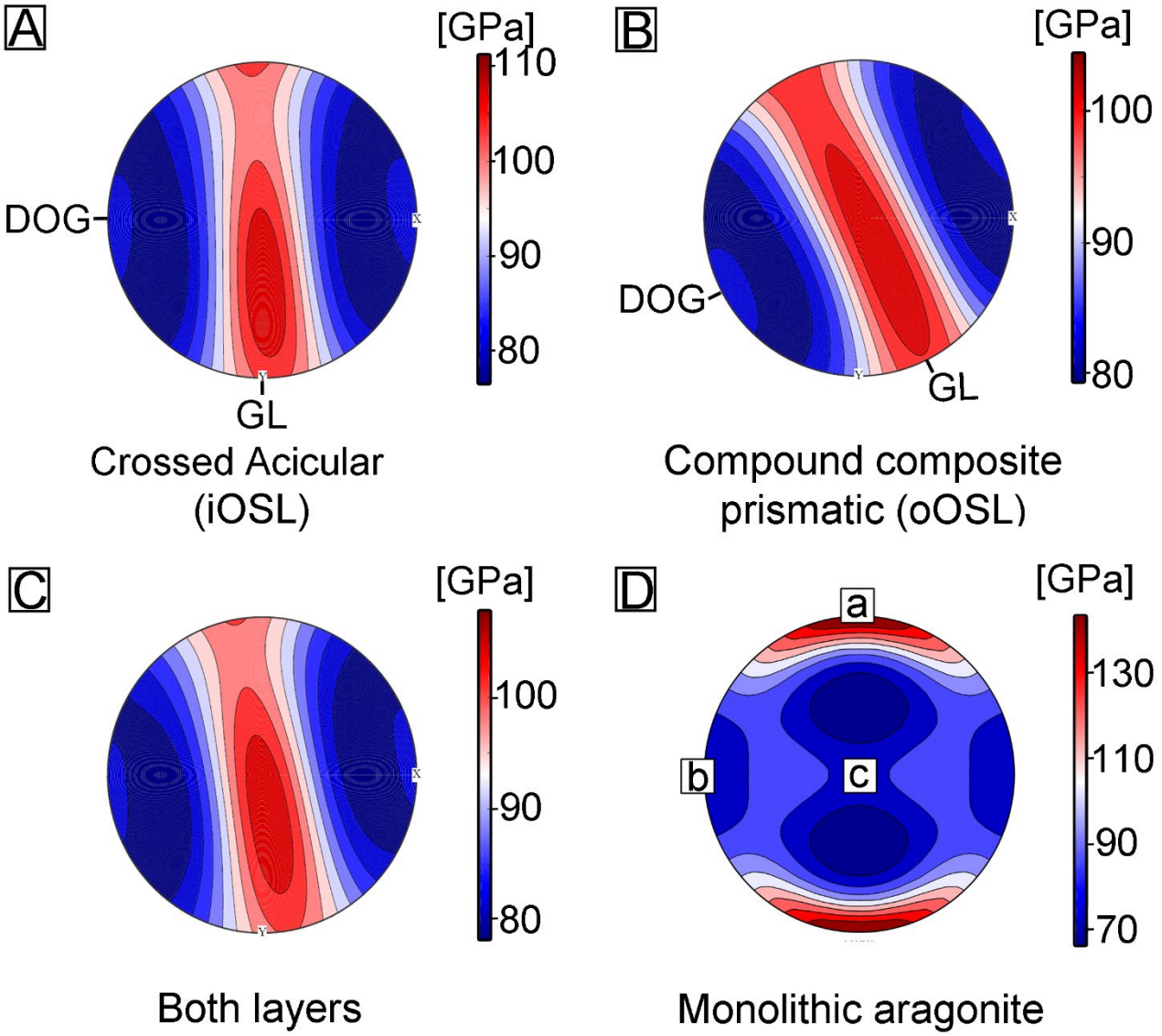

Figure 7: Young's moduli (upper hemisphere and equal area projection), for the compound composite prismatic (oOSL, A) and crossed-acicular ultrastructure (iOSL, B) as well as for both layers together (C). Calculations were made with the Hill averaging scheme (colour scale on the right). (D) The Young's modulus for a aragonite single crystal is calculated with the Voigt–Reuss–Hill averaging scheme and is based on the elastic constants published in De Villiers (1971). We used the aragonite single crystal elastic properties of Pavese et al. (1992) and the EBSD data collected from *K. rhytiphora* from this study as inputs (GL – local growth line, DOG – local direction of growth. Note the reference frame for (D) is given by the aragonite crystallographic axes.

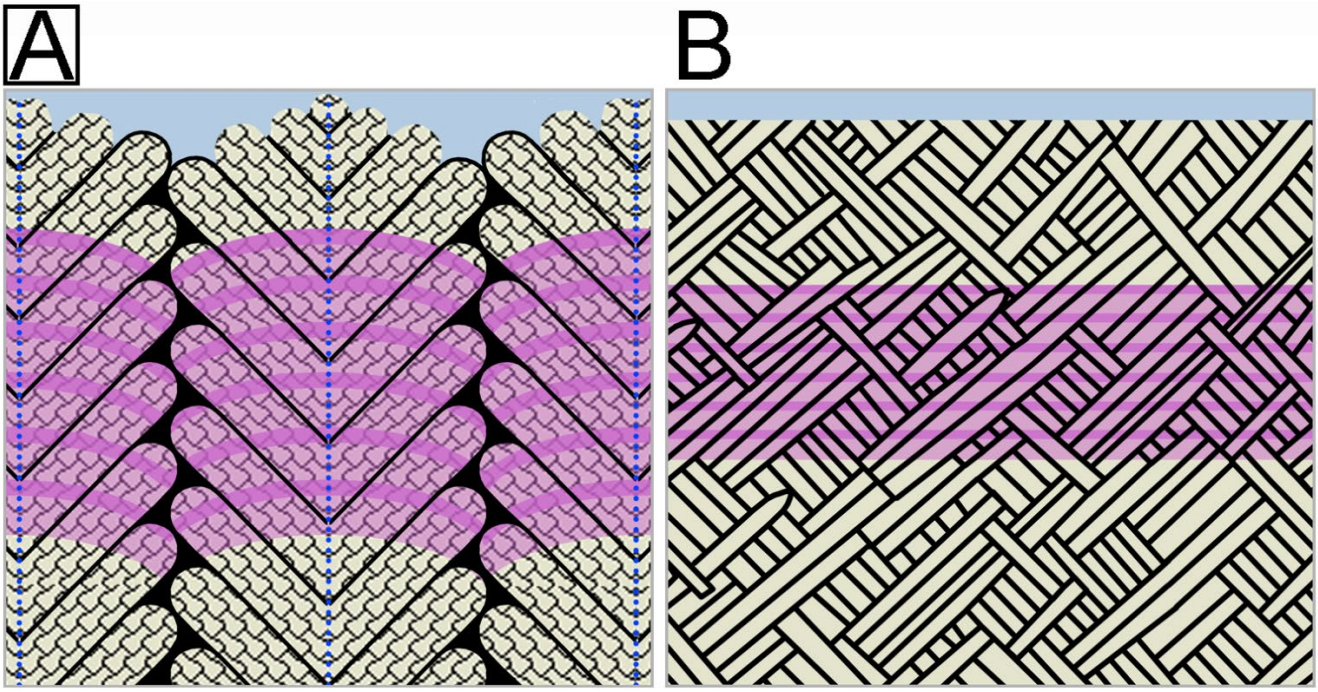

Figure 8: Schematic (not to scale) of the compound composite prismatic (oOSL, A) and crossed-acicular architecture (iOSL, B; modified after Bandel, 1977) transected by Sr-labels (purple) summarizing the observations in this study. Unlabelled aragonitic architectural units (beige) are outlined by organic sheaths (black). First-order prisms in (A) have thick organic sheaths, curved growth fronts, and consist of second-order prisms that are arranged at ca. 60° to the central axis of each first-order prism (A, blue dashed lines). Third-order prisms (A, tiled pattern) are oriented parallel to each other within second-order prisms. The shading in the pink Sr labels illustrates the internal BSE greyscale variations in the Sr labels reflecting variable Sr-concentrations within the Sr-label in the shells. The Sr-label is generally wider in the oOSL compared to the iOSL and transects all architectural units in both ultrastructures.

Tables

Table 1: Geochemical composition of *K. rhytiphora* obtained from wavelength-dispersive X-ray spectrometry (WDS) electron probe micro analyser (EPMA) provided as µg·g^{-1} averages (Avg.) and standard deviations (Stdev.) as well as molar element/Ca ratios for shell compositions grown under different conditions in the wild ("pre-aqua"), in aquaculture during pulsed Sr-labelling ("LE 1" and "LE 2"), and non-labelling ("pre-NE 1" and "NE 1") periods.

			Na	Mg	S	Cl	Ca	Sr	Na/Ca	Mg/Ca	Sr/Ca
Compound composite prismatic	**Pre-Aqua**	**Avg.**	**5,300**	**180**	**400**	**400**	**389,000**	**1,000**	**23.95**	**0.77**	**1.19**
	(n=5)	Stdev	450	120	160	100	1,400	300	2.00	0.51	0.30
	Pre-LE 1	**Avg.**	**4,200**	**240**	**560**	**400**	**391,000**	**1,100**	**18.84**	**1.02**	**1.29**
	(n=3)	Stdev	300	60	120	100	500	90	1.32	0.25	0.10
	LE 1	**Avg.**	**4,200**	**240**	**480**	**300**	**378,000**	**20,000**	**19.17**	**1.05**	**24.16**
	(n=3)	Stdev	300	60	80	100	600	600	1.37	0.26	0.72
	NE 1	**Avg.**	**3,000**	**180**	**680**	**300**	**391,000**	**1,350**	**13.56**	**0.76**	**1.58**
	(n=3)	Stdev	70	180	200	200	3,100	90	0.33	0.76	0.10
	LE 2	**Avg.**	**4,800**	**240**	**480**	200	**385,000**	**19,000**	**21.86**	**1.03**	**23.04**
	(n=3)	Stdev	300	60	120	100	1,100	200	1.35	0.26	0.20
Crossed-Acicular*	**Pre-Aqua**	**Avg.**	**5,600**	**bdl**	**200**	**200**	**386,000**	**900**	**25.12**	**bdl**	**1.10**
	(n=5)	Stdev	670	-	240	100	400	300	3.01	-	0.40
	Pre-LE 1	**Avg.**	**5,700**	**bdl**	**200**	**200**	**384,000**	**900**	**25.91**	**bdl**	**1.01**
	(n=3)	Stdev	670	-	120	200	500	300	3.03	-	0.40
	LE 1	**Avg.**	**5,600**	**bdl**	**520**	**300**	**380,000**	**>12,000**	**25.52**	**bdl**	**>14.55**
	(n=3)	Stdev	670	-	280	100	400	300	3.06	-	0.41
	NE 1	**Avg.**	**5,300**	**180**	**800**	**200**	**390,000**	**1,300**	**23.89**	**0.77**	**1.49**
	(n=3)	Stdev	670	300	280	200	400	300	2.99	1.28	0.40
	Limits of Detection:		400	100	100	100	300	200	-	-	-

Mn, Ba, P, K, and Fe, were analysed and were always below detection limits (200 µg·g^{-1} for Mn, Ba, Fe and 100 µg·g^{-1} for P, K). *LE2 and NE 2 in the crossed-acicular ultrastructure (iOSL) were too close to the edge and are excluded, LE1 is a minimum value as the analysed area slightly exceeds label width. See Table S2 for data in wt.% (g·g^{-1}) oxide.

Table 2: Average daily local growth rates from pulsed Sr-labelling experiments. Rates in bold in NE2 were formed within 6 days (K2-01 to K2-04), all other rates in this column are within 12 days (K2-06 to K2-11). Average daily local growth rates for the entire experimental period are 0.85 (oOSL) and 0.73 µm (iOSL) For full details lists of all measurements see Tables S3 and S4.

Sample ID:	Shell layer	LE 1 [µm/d]	NE 1 [µm/d]	LE 2 [µm/d]	NE 2 [µm/d]	Total growth period [**µm/30d**], [µm/36d]	Daily growth period [µm/d]
K2-01*	oOSL	0.85 ± 0.10	0.48 ± 0.05	n.a.	n.a.	**10.8 ± 1.1**	0.66 ± 0.08
	iOSL	0.58 ± 0.03	0.31 ± 0.03	0.67 ± 0.03	*0.55 ± 0.03*	**14.5 ± 0.9**	0.53 ± 0.03
K2-02	oOSL	0.37 ± 0.07	0.31 ± 0.04	0.43 ± 0.08	*0.47 ± 0.05*	**11.3 ± 1.6**	0.39 ± 0.08
	iOSL	0.60 ± 0.05	0.36 ± 0.03	0.65 ± 0.03	*0.43 ± 0.05*	**14.4 ± 1.1**	0.45 ± 0.05
K2-04	oOSL	2.22 ± 0.15	1.67 ± 0.05	0.80 ± 0.12	*0.97 ± 0.13*	**43.9 ± 2.9**	1.41 ± 0.15
	iOSL	1.17 ± 0.32	0.85 ± 0.08	0.72 ± 0.07	*0.43 ± 0.12*	**24.0 ± 3.9**	0.79 ± 0.17
K2-06	oOSL	0.63 ± 0.20	0.88 ± 0.14	0.58 ± 0.12	1.03 ± 0.13	30.1 ± 1.3	0.78 ± 0.12
	iOSL	1.00 ± 0.10	1.13 ± 0.05	0.92 ± 0.03	0.84 ± 0.03	35.1 ± 1.8	0.97 ± 0.05
K2-08	oOSL	1.07 ± 0.30	1.86 ± 0.13	0.58 ± 0.15	1.41 ± 0.04	49.2 ± 1.2	1.23 ± 0.13
	iOSL	0.87 ± 0.08	0.89 ± 0.03	0.62 ± 0.05	0.61 ± 0.03	26.9 ± 1.4	0.75 ± 0.08
K2-11	oOSL	0.46 ± 0.12	0.90 ± 0.11	0.60 ± 0.15	0.64 ± 0.11	24.9 ± 4.2	0.65 ± 0.11
	iOSL	1.12 ± 0.05	0.97 ± 0.17	0.73 ± 0.03	0.63 ± 0.03	30.3 ± 0.9	0.86 ± 0.02
	Av. oOSL	**0.93 ± 0.15**	**1.02 ± 0.09**	**0.60 ± 0.12**	**0.76 ± 0.08**	**28.4 ± 2.1**	**0.85 ± 0.11**
	Av. iOSL	**0.88 ± 0.10**	**0.75 ± 0.04**	**0.72 ± 0.05**	**0.47 ± 0.03**	**24.2 ± 1.7**	**0.73 ± 0.07**

*This individual did not show prismatic growth after NE1, while the crossed-acicular ultrastructure kept growing.

Table 3: Distribution coefficients of Ca and Sr between shell and seawater for both ultrastructures as well as for pulse Sr-labelled and unlabelled conditions. Concentrations for Ca and Sr in shell are from Table 1, while seawater values are mean ocean water.

Distribution coefficients:	Compound composite prismatic (oOSL) ultrastructure	Crossed-acicular (iOSL) ultrastructure
D_{Sr} labelled $(Sr/Ca_{\text{labelled shell}})/(Sr/Ca_{\text{seawater}})$	0.15	>0.09*
D_{Sr} unlabelled $(Sr/Ca_{\text{unlabelled shell}}/(Sr/Ca_{\text{seawater}})$	0.14	0.14
D_{Sr} natural environment $(Sr/Ca_{\text{natural shell}}/(Sr/Ca_{\text{seawater}})$	0.13	0.12

*Minimum value as the analysed area slightly exceeds label width.

References

Addadi, L., Joester, D., Nudelman, F., and Weiner, S.: Mollusk shell formation: a source of new concepts for understanding biomineralization processes, Chemistry–A European Journal, 12, 980–987, 2006.

Agbaje, O. B. A., Thomas, D. E., Mclnerney, B. V., Molloy, M. P., and Jacob, D. E.: Organic macromolecules in shells of Arctica islandica: Comparison with nacroprismatic bivalve shells, Marine Biology, 164, 1-13, 2017a.

Agbaje, O. B.A., Wirth, R., Morales, L. F.G., Shirai, K., Kosnik, M., Watanabe, T., and Jacob, D. E.: Architecture of crossed-lamellar bivalve shells: The southern giant clam (Tridacna derasa, Röding, 1798), Royal Society Open Science, 4, 1–15, 2017b.

Alia, J. M., Mera, Y. D. de, Edwards, H. G.M., Martín, P. G., and Andres, S. L.: FT-Raman and infrared spectroscopic study of aragonite-strontianite (CaxSr1− xCO3) solid solution, Spectrochimica Acta Part A: Molecular and Biomolecular Spectroscopy, 53, 2347–2362, 1997.

Allison, N., Cohen, I., Finch, A. A., and Erez, J.: Controls on Sr/Ca and Mg/Ca in scleractinian corals: The effects of Ca-ATPase and transcellular Ca channels on skeletal chemistry, Geochimica et Cosmochimica Acta, 75, 6350–6360, 2011.

Almagro, I., Drzymała, P., Berent, K., Sainz-Díaz, C. I., Willinger, M. G., Bonarski, J., and Checa, A. G.: New crystallographic relationships in biogenic aragonite: The crossed-lamellar microstructures of mollusks, Crystal Growth & Design, 16, 2083–2093, 2016.

Bachmann, F., Hielscher, R., Jupp, P. E., Pantleon, W., Schaeben, H., and Wegert, E.: Inferential statistics of electron backscatter diffraction data from within individual crystalline grains, Journal of Applied Crystallography, 43, 1338–1355, 2010.

Bailey, T. R. and Lear, C. H.: Testing the effect of carbonate saturation on the Sr/Ca of biogenic aragonite: A case study from the River Ehen, Cumbria, UK, Geochemistry, Geophysics, Geosystems, 7, 1–6, 2006.

Bevelander, G. and Nakahara, H.: An electron microscope study of the formation of the nacreous layer in the shell of certain bivalve molluscs, Calcified Tissue Research, 3, 84–92, 1969.

Bischoff, W. D., Sharma, S. K., and MacKenzie, F. T.: Carbonate ion disorder in synthetic and biogenic magnesian calcites: A Raman spectral study, American Mineralogist, 70, 581–589, 1985.

Böhm, C. F., Demmert, B., Harris, J., Fey, T., Marin, F., and Wolf, S. E.: Structural commonalities and deviations in the hierarchical organization of crossed-lamellar shells: A case study on the shell of the bivalve Glycymeris glycymeris, Journal of Materials Research, 31, 536–546, 2016.

Cann, J. H., Deckker, P. de, and Murray-Wallace, C. V.: Coastal aboriginal shell middens and their palaeoenvironmental significance, Robe Range, South Australia, Transactions of the Royal Society of South Australia, 115, 161–175, 1991.

Carré, M., Bentaleb, I., Blamart, D., Ogle, N., Cardenas, F., Zevallos, S., Kalin, R. M., Ortlieb, L., and Fontugne, M.: Stable isotopes and sclerochronology of the bivalve Mesodesma donacium: Potential application to Peruvian paleoceanographic reconstructions, Palaeogeography, Palaeoclimatology, Palaeoecology, 228, 4–25, 2005.

Carré, M., Bentaleb, I., Bruguier, O., Ordinola, E., Barrett, N. T., and Fontugne, M.: Calcification rate influence on trace element concentrations in aragonitic bivalve shells: Evidences and mechanisms, Geochimica et Cosmochimica Acta, 70, 4906–4920, 2006.

Carter, J. G.: Skeletal biomineralization: patterns, processes and evolutionary trends, 1, American Geophysical Union, 700 pp., 1989.

Carteret, C., La Pierre, M. de, Dossot, M., Pascale, F., Erba, A., and Dovesi, R.: The vibrational spectrum of CaCO3 aragonite: A combined experimental and quantum-mechanical investigation, The Journal of Chemical Physics, 138, 14201, 2013.

Chateigner, D., Hedegaard, C., and Wenk, H.-R.: Mollusc shell microstructures and crystallographic textures, Journal of Structural Geology, 22, 1723–1735, 2000.

Checa, A. G., Cartwright, J. H. E., and Willinger, M.-G.: Mineral bridges in nacre, Journal of Structural Biology, 176, 330–339, 2011.

Checa, A. G., Okamoto, T., and Ramírez, J.: Organization pattern of nacre in Pteriidae (Bivalvia: Mollusca) explained by crystal competition, Proceedings of the Royal Society of London B: Biological Sciences, 273, 1329–1337, 2006.

Currey, J. D. and Kohn, A. J.: Fracture in the crossed-lamellar structure of Conus shells, Journal of Materials Science, 11, 1615–1623, 1976.

Cusack, M., Parkinson, D., Freer, A., Perez-Huerta, A., Fallick, A. E., and Curry, G. B.: Oxygen isotope composition in Modiolus modiolus aragonite in the context of biological and crystallographic control, Journal of Mineral Science, 72, 569–577, 2008.

Dauphin, Y., Brunelle, A., Medjoubi, K., Somogyi, A., and Cuif, J.-P.: The Prismatic Layer of Pinna: A Showcase of Methodological Problems and Preconceived Hypotheses, Minerals, 8, 365, 2018.

de Yoreo, J. J., Gilbert, P.U.P.A., Sommerdijk, N. A., Penn, R. L., Whitelam, S., Joester, D., Zhang, H., Rimer, J. D., Navrotsky, A., and Banfield, J. F.: Crystallization by particle attachment in synthetic, biogenic, and geologic environments, Science, 349, 1-9, 2015.

Dodd, J. R.: Environmental control of strontium and magnesium in Mytilus, Geochimica et Cosmochimica Acta, 29, 385–398, 1965.

Domart-Coulon, I., Stolarski, J., Brahmi, C., Gutner-Hoch, E., Janiszewska, K., Shemesh, A., and Meibom, A.: Simultaneous extension of both basic microstructural components in scleractinian coral skeleton during night and daytime, visualized by in situ 86 Sr pulse labeling, Journal of Structural Biology, 185, 79–88, 2014.

Edgar, G. J.: Australian marine life: The plants and animals of temperate waters, Rev. ed., Reed New Holland, Frenchs Forest, N.S.W., London, 544 pp., 2000.

Evans, J. W.: Tidal growth increments in the cockle Clinocardium nuttalli, Science, 176, 416–417, 1972.

Fitzer, S. C., Vittert, L., Bowman, A., Kamenos, N. A., Phoenix, V. R., and Cusack, M.: Ocean acidification and temperature increase impact mussel shell shape and thickness: problematic for protection?, Ecology and Evolution, 5, 4875–4884, 2015.

Foster, L. C., Allison, N., Finch, A. A., and Andersson, C.: Strontium distribution in the shell of the aragonite bivalve Arctica islandica, Geochemistry, Geophysics, Geosystems, 10, 1–14, 2009.

Gaetani, G. A. and Cohen, A. L.: Element partitioning during precipitation of aragonite from seawater: A framework for understanding paleoproxies, Geochimica et Cosmochimica Acta, 70, 4617–4634, 2006.

Gilbert, P.U.P.A., Metzler, R. A., Zhou, D., Scholl, A., Doran, A., Young, A., Kunz, M., Tamura, N., and Coppersmith, S. N.: Gradual ordering in red abalone nacre, Journal of the American Chemical Society, 130, 17519–17527, 2008.

Gillikin, D. P., Lorrain, A., Navez, J., Taylor, J. W., André, L., Keppens, E., Baeyens, W., and Dehairs, F.: Strong biological controls on Sr/Ca ratios in aragonitic marine bivalve shells, Geochemistry, Geophysics, Geosystems, 6, 1–16, 2005.

Gillikin, D. P., Lorrain, A., Paulet, Y.-M., André, L., and Dehairs, F.: Synchronous barium peaks in high-resolution profiles of calcite and aragonite marine bivalve shells, Geo-Marine Letters, 28, 351–358, 2008.

Goldstein, J. I., Newbury, D. E., Michael, J. R., Ritchie, N. W. M., Scott, J. H. J., and Joy, D. C.: Scanning electron microscopy and X-ray microanalysis, Springer, 2017.

Gorzelak, P., Stolarski, J., Dery, A., Dubois, P., Escrig, S., and Meibom, A.: Ultrascale and microscale growth dynamics of the cidaroid spine of Phyllacanthus imperialis revealed by 26Mg labeling and NanoSIMS isotopic imaging, Journal of Morphology, 275, 788–796, 2014.

Gutner-Hoch, E., Schneider, K., Stolarski, J., Domart-Coulon, I., Yam, R., Meibom, A., Shemesh, A., and Levy, O.: Evidence for Rhythmicity Pacemaker in the Calcification Process of Scleractinian Coral, Scientific Reports, 6, 1–8, 2016.

Hallmann, N., Burchell, M., Schöne, B. R., Irvine, G. V., and Maxwell, D.: High-resolution sclerochronological analysis of the bivalve mollusk Saxidomus gigantea from Alaska and British Columbia: Techniques for revealing environmental archives and archaeological seasonality, Journal of Archaeological Science, 36, 2353–2364, 2009.

Hashin, Z.: The elastic moduli of heterogeneous materials, Journal of Applied Mechanics, 29, 143–150, 1962.

Henry, H., Tilhac, R., Griffin, W. L., O'Reilly, S. Y., Satsukawa, T., Kaczmarek, M.-A., Grégoire, M., and Ceuleneer, G.: Deformation of mantle pyroxenites provides clues to geodynamic processes in subduction zones: Case study of the Cabo Ortegal Complex, Spain, Earth and Planetary Science Letters, 472, 174–185, 2017.

Jackson, A. P., Vincent, J. F.V., and Turner, R. M.: The mechanical design of nacre, Proceedings of the Royal Society of London B: Biological Sciences, 234, 415–440, 1988.

Jacob, D. E., Soldati, A. L., Wirth, R., Huth, J., Wehrmeister, U., and Hofmeister, W.: Nanostructure, composition and mechanisms of bivalve shell growth, Geochimica et Cosmochimica Acta, 72, 5401–5415, 2008.

Jacob, D. E., Wirth, R., Agbaje, O. B.A., Branson, O., and Eggins, S. M.: Planktic foraminifera form their shells via metastable carbonate phases, Nature Communications, 8, 1–9, 2017.

Kamat, S., Su, X., Ballarini, R., and Heuer, A. H.: Structural basis for the fracture toughness of the shell of the conch Strombus gigas, Nature, 405, 1036–1040, 2000.

Katti, K. S., Mohanty, B., and Katti, D. R.: Nanomechanical properties of nacre, Journal of Materials Research, 21, 1237–1242, 2006.

Klein, R. T., Lohmann, K. C., and Thayer, C. W.: Bivalve skeletons record sea-surface temperature and δ18O via Mg/Ca and 18O/16O ratios, Geology, 24, 415–418, 1996a.

Klein, R. T., Lohmann, K. C., and Thayer, C. W.: SrCa and 13C12C ratios in skeletal calcite of Mytilus trossulus: Covariation with metabolic rate, salinity, and carbon isotopic composition of seawater, Geochimica et Cosmochimica Acta, 60, 4207–4221, 1996b.

Kobayashi, I. and Akai, J.: Twinned aragonite crystals found in the bivalvian crossed lamellar shell structure, The Journal of the Geological Society of Japan, 100, 177–180, 1994.

Levi-Kalisman, Y., Falini, G., Addadi, L., and Weiner, S.: Structure of the nacreous organic matrix of a bivalve mollusk shell examined in the hydrated state using cryo-TEM, Journal of Structural Biology, 135, 8–17, 2001.

Liu, L.-G., Chen, C.-C., Lin, C.-C., and Yang, Y.-J.: Elasticity of single-crystal aragonite by Brillouin spectroscopy, Physics and Chemistry of Minerals, 32, 97–102, 2005.

Mainprice, D., Hielscher, R., and Schaeben, H.: Calculating anisotropic physical properties from texture data using the MTEX open-source package, Geological Society, London, Special Publications, 360, 175–192, 2011.

Marin, F., Le Roy, N., and Marie, B.: The formation and mineralization of mollusk shell, Frontiers in Bioscience, 4, 1099–1125, 2012.

Nehrke, G., Keul, N., Langer, G., Nooijer, L. J. de, Bijma, J., and Meibom, A.: A new model for biomineralization and trace-element signatures of Foraminifera tests, Biogeosciences, 10, 6759–6767, 2013.

Nell, J. A., O'Connor, W. A., Heasman, M. P., and Goard, L. J.: Hatchery production for the venerid clam Katelysia rhytiphora (Lamy) and the Sydney cockle Anadara trapezia (Deshayes), Aquaculture, 119, 149–156, 1994.

Nell, J. A. and Paterson, K. J.: Salinity studies on the clams Katelysia rhytiphora (Lamy) and Tapes dorsatus (Lamarck), Aquaculture Research, 28, 115–119, 1997.

Nudelman, F.: Nacre biomineralisation: A review on the mechanisms of crystal nucleation, Seminars in Cell & Developmental Biology, 46, 2–10, 2015.

O'Donnell, M. D., Fredholm, Y., Rouffignac, A. de, and Hill, R. G.: Structural analysis of a series of strontium-substituted apatites, Acta Biomaterialia, 4, 1455–1464, 2008.

Otter, L. M., Agbaje, O., Le Huong, T.-T., Häger, T., and Jacob, D. E.: Akoya Cultured Pearl Farming in Eastern Australia, Gems & Gemology, 53, 423–437, 2017.

Pannella, G. and MacClintock, C.: Biological and environmental rhythms reflected in molluscan shell growth, Journal of Paleontology, 42, 64–80, 1968.

Pérez-Huerta, A., Cuif, J.-P., Dauphin, Y., and Cusack, M.: Crystallography of calcite in pearls, European Journal of Mineralogy, 26, 507–516, 2014.

Popov, S. V.: Composite prismatic structure in bivalve shell, Acta Palaeontologica Polonica, 31, 3–26, 1986.

Purton, L. M. A., Shields, G. A., Brasier, M. D., and Grime, G. W.: Metabolism controls Sr/Ca ratios in fossil aragonitic mollusks, Geology, 27, 1083–1086, 1999.

Radermacher, P., Schöne, B. R., Gischler, E., Oschmann, W., Thébault, J., and Fiebig, J.: Sclerochronology–a highly versatile tool for mariculture and reconstruction of life history traits of the queen conch, Strombus gigas (Gastropoda), Aquatic Living Resources, 22, 307–318, 2009.

Rhoads, D. C. and Lutz, R. A.: Skeletal Growth of Aquatic Organisms: Biological records of environmental change, Plenum Press, 750 pp., 1980.

Rodriguez-Navarro, A. B., Checa, A., Willinger, M.-G., Bolmaro, R., and Bonarski, J.: Crystallographic relationships in the crossed lamellar microstructure of the shell of the gastropod Conus marmoreus, Acta Biomaterialia, 8, 830–835, 2012.

Ropes, J. W., Jones, D. S., Murawski, S. A., Serchuk, F. M., and Jearld, A.: Documentation of annual growth lines in ocean quahogs, Arctica islandica Linne, Fishery Bulletin, 82, 1–19, 1984.

Rousseau, M., Meibom, A., Gèze, M., Bourrat, X., Angellier, M., and Lopez, E.: Dynamics of sheet nacre formation in bivalves, Journal of Structural Biology, 165, 190–195, 2009.

Ruschel, K., Nasdala, L., Kronz, A., Hanchar, J. M., Többens, D. M., Škoda, R., Finger, F., and Möller, A.: A Raman spectroscopic study on the structural disorder of monazite–(Ce), Mineralogy and Petrology, 105, 41–55, 2012.

Russell, M. P. and Urbaniak, L. M. (Eds.): Does calcein affect estimates of growth rates in sea urchins?, CRC Press, 53 pp., 2004.

Sand, K. K., Pedersen, C. S., Matthiesen, J., Dobberschütz, S., and Stipp, S. L.S.: Controlling biomineralisation with cations, Nanoscale, 9, 12925–12933, 2017.

Schindelin, J., Rueden, C. T., Hiner, M. C., and Eliceiri, K. W.: The ImageJ ecosystem: An open platform for biomedical image analysis, Molecular Reproduction and Development, 82, 518–529, 2015.

Schoeppler, V., Gránásy, L., Reich, E., Poulsen, N., Kloe, R. de, Cook, P., Rack, A., Pusztai, T., and Zlotnikov, I.: Biomineralization as a Paradigm of Directional Solidification: A Physical Model for Molluscan Shell Ultrastructural Morphogenesis, Advanced Materials, 30, 1–8, 2018.

Schöne, B. R.: The curse of physiology—challenges and opportunities in the interpretation of geochemical data from mollusk shells, Geo-Marine Letters, 28, 269–285, 2008.

Schöne, B. R., Fiebig, J., Pfeiffer, M., Gleβ, R., Hickson, J., La Johnson, A., Dreyer, W., and Oschmann, W.: Climate records from a bivalved Methuselah (Arctica islandica, Mollusca; Iceland), Palaeogeography, Palaeoclimatology, Palaeoecology, 228, 130–148, 2005.

Schöne, B. R., Goodwin, D. H., Flessa, K. W., and Dettman, D. L.: Sclerochronology and Growth of the Bivalve Mollusks Chione (Chionista) fluctifraga and C.(Chionista) cortezi, the Veliger, 45, 45–54, 2002.

Schöne, B. R., Zhang, Z., Radermacher, P., Thébault, J., Jacob, D. E., Nunn, E. V., and Maurer, A.-F.: Sr/Ca and Mg/Ca ratios of ontogenetically old, long-lived bivalve shells (Arctica islandica) and their function as paleotemperature proxies, Palaeogeography, Palaeoclimatology, Palaeoecology, 302, 52–64, 2011.

Shimamoto, M.: Shell microstructure of the Veneridae (Bivalvia) and its phylogenetic implications, 東北大學理科報告. 地質學, 56, 1-40, 1986.

Shirai, K., Sowa, K., Watanabe, T., Sano, Y., Nakamura, T., and Clode, P.: Visualization of sub-daily skeletal growth patterns in massive Porites corals grown in Sr-enriched seawater, Journal of Structural Biology, 180, 47–56, 2012.

Simkiss, K.: The organic matrix of the oyster shell, Comparative Biochemistry and Physiology, 16, 427–435, 1965.

Stephenson, A. E., DeYoreo, J. J., Wu, L., Wu, K. J., Hoyer, J., and Dove, P. M.: Peptides enhance magnesium signature in calcite: Insights into origins of vital effects, Science, 322, 724–727, 2008.

Swan, E. F.: The meaning of strontium-calcium ratios, Deep-Sea Research, 4, 71, 1956.

Takesue, R. K. and van Geen, A.: Mg/Ca, Sr/Ca, and stable isotopes in modern and Holocene Protothaca staminea shells from a northern California coastal upwelling region, Geochimica et Cosmochimica Acta, 68, 3845–3861, 2004.

Taylor, J. D.: The shell structure and mineralogy of the Bivalvia. Introduction. Nuculacea-Trigonacea, Bulletin of the British Museum (Natural History). Zoology, 3, 1–125, 1969.

Thébault, J., Chauvaud, L., Clavier, J., Fichez, R., and Morize, E.: Evidence of a 2-day periodicity of striae formation in the tropical scallop Comptopallium radula using calcein marking, Marine Biology, 149, 257–267, 2006.

Urey, H. C., Lowenstam, H. A., Epstein, S., and McKinney, C. R.: Measurement of paleotemperatures and temperatures of the Upper Cretaceous of England, Denmark, and the southeastern United States, Geological Society of America Bulletin, 62, 399–416, 1951.

Urmos, J., Sharma, S. K., and Mackenzie, F. T.: Characterization of some biogenic carbonates with Raman spectroscopy, American Mineralogist, 76, 641–646, 1991.

Váczi, T.: A new, simple approximation for the deconvolution of instrumental broadening in spectroscopic band profiles, Applied Spectroscopy, 68, 1274–1278, 2014.

Wang, D., Wallace, A. F., Yoreo, J. J. de, and Dove, P. M.: Carboxylated molecules regulate magnesium content of amorphous calcium carbonates during calcification, Proceedings of the National Academy of Sciences, 106, 21511–21516, 2009.

Wang, R. Z., Suo, Z., Evans, A. G., Yao, N., and Aksay, I. A.: Deformation mechanisms in nacre, Journal of Materials Research, 16, 2485–2493, 2001.

Wehrmeister, U., Soldati, A. L., Jacob, D. E., Häger, T., and Hofmeister, W.: Raman spectroscopy of synthetic, geological and biological vaterite: a Raman spectroscopic study, Journal of Raman Spectroscopy, 41, 193–201, 2010.

Weiner, S., Addadi, L., and Wagner, H. D.: Materials design in biology, Materials Science and Engineering: C, 11, 1–8, 2000.

Weiner, S. and Traub, W.: X-ray diffraction study of the insoluble organic matrix of mollusk shells, FEBS Letters, 111, 311–316, 1980.

Weiner, S., Traub, W., and Parker, S. B.: Macromolecules in mollusc shells and their functions in biomineralization [and Discussion], Philosophical Transactions of the Royal Society of London B: Biological Sciences, 304, 425–434, 1984.

Wolf, S. E., Böhm, C. F., Harris, J., Demmert, B., Jacob, D. E., Mondeshki, M., Ruiz-Agudo, E., and Rodriguez-Navarro, C.: Nonclassical Crystallization in vivo et in vitro (I): Process-Structure-Property relationships of nanogranular biominerals, Journal of Structural Biology, 196, 244–259, 2016.

Wolf, S. E., Lieberwirth, I., Natalio, F., Bardeau, J.-F., Delorme, N., Emmerling, F., Barrea, R., Kappl, M., and Marin, F.: Merging models of biomineralisation with concepts of nonclassical crystallisation: Is a liquid amorphous precursor involved in the formation of the prismatic layer of the Mediterranean Fan Mussel Pinna nobilis?, Faraday Discussions, 159, 433–448, 2012.

Zhao, L., Schöne, B. R., and Mertz-Kraus, R.: Controls on strontium and barium incorporation into freshwater bivalve shells (Corbicula fluminea), Palaeogeography, Palaeoclimatology, Palaeoecology, 465, 386–394, 2017a.

Zhao, L., Schöne, B. R., Mertz-Kraus, R., and Yang, F.: Insights from sodium into the impacts of elevated pCO 2 and temperature on bivalve shell formation, Journal of Experimental Marine Biology and Ecology, 486, 148–154, 2017b.